Antibody-mediated targeting of TNFR2 activates CD8$^+$ T cells in mice and promotes antitumor immunity

Eric M. Tam[1]*†, Ross B. Fulton[1]*, James F. Sampson[1]*, Marco Muda[1], Adam Camblin[1], Jennifer Richards[1], Alexander Koshkaryev[1], Jian Tang[1], Vinodh Kurella[1], Yang Jiao[1], Lihui Xu[1], Kathy Zhang[1], Neeraj Kohli[1], Lia Luus[1], Elizabeth Hutto[2], Sandeep Kumar[1], James Lulo[1], Violette Paragas[1], Christina Wong[1], James Suchy[1], Stephanie Grabow[1], Anne-Sophie Dugast[1], Hong Zhang[1], Fabien Depis[1], Sonia Feau[1], Aniela Jakubowski[1], Wenlian Qiao[1], Galina Craig[1], Maja Razlog[1], James Qiu[1], Yu Zhou[3], James D. Marks[3], Michael Croft[4,5], Daryl C. Drummond[1], Andreas Raue[1†]

Tumor necrosis factor receptor 2 (TNFR2) is the alternate receptor for TNF and can mediate both pro- and anti-inflammatory activities of T cells. Although TNFR2 has been linked to enhanced suppressive activity of regulatory T cells (T_{regs}) in autoimmune diseases, the viability of TNFR2 as a target for cancer immunotherapy has been underappreciated. Here, we show that new murine monoclonal anti-TNFR2 antibodies yield robust antitumor activity and durable protective memory in multiple mouse cancer cell line models. The antibodies mediate potent Fc-dependent T cell costimulation and do not result in significant depletion of T_{regs}. Corresponding human agonistic monoclonal anti-TNFR2 antibodies were identified and also had antitumor effects in humanized mouse models. Anti-TNFR2 antibodies could be developed as a novel treatment option for patients with cancer.

INTRODUCTION

Programmed cell death protein 1 (PD-1) and cytotoxic T lymphocyte associated protein 4 (CTLA-4) checkpoint inhibitors have offered substantial promise in the treatment of cancer (*1*, *2*). Unfortunately, their activity remains limited to a subset of patients in indications such as metastatic bladder cancer, non–small cell lung cancer (NSCLC), melanoma, and head and neck cancers, with many progressing over time (*3*–*5*). Anti–PD-1 combinations with chemotherapy or other immunotherapies, such as anti–CTLA-4, have been able to improve efficacy, but often at the expense of substantial increases in toxicities compared to anti–PD-1 alone (*6*, *7*). Consequently, there is an ongoing need for new cancer immunotherapies that have promising activity, but that are also well tolerated.

The pleiotropic cytokine tumor necrosis factor (TNF) mediates immune and inflamatory responses through binding of two receptors: TNF receptor 1 (TNFR1) and TNFR2. In contrast to the ubiquitously expressed TNFR1, TNFR2 is expressed primarily on immune cells, as reviewed in (*8*). Whereas both receptors share binding to TNF and lymphotoxin (LT-α) (*9*), TNFR2 is primarily activated by transmembrane TNF (*10*, *11*). Although the pathways and functional outcomes for TNF signaling via TNFR1 are well characterized (*12*), much less is known about TNFR2 signaling. TNFR2 is expressed on activated but not on resting T cells and, therefore, is likely to be expressed primarily by T cells in a tumor where an active immune response is ongoing. Most recently, TNFR2 has been described to be expressed more highly by regulatory T cells (T_{regs}) than conventional T cells and to support T_{reg} growth or survival, leading to the hypothesis that manipulation of this receptor could be beneficial in cancer (*13*–*15*). Accordingly, TNFR2 knockout mice were found to exhibit decreased tumor growth while tumor burden was unaffected in TNFR1 knockout mice (*16*).

Monoclonal antibodies (mAbs) targeting TNFR2 have already been described to have limited antitumor activity in syngeneic tumor models (*15*). However, the principal mechanism was unclear as the antibodies were described to block TNF binding but, when clustered, are also able to induce nuclear factor κB (NFκB) signaling through TNFR2. More recently, in vitro studies have shown that targeting TNFR2 with antagonistic antibodies inhibits proliferation of ovarian cancer cells and tumor-associated T_{regs} (*17*) and that TNFR2-expressing tumor cells and T_{regs} are killed by TNFR2 antagonistic antibodies in advanced Sézary syndrome (*18*). In autoimmune models, TNFR2 signaling has been shown to promote T_{reg} function and mediate disease protection (*19*, *20*). Although anti-TNFR2–based therapy has been discussed as a possible treatment for cancer (*21*–*24*), it is unclear whether it would be preferential to develop an antagonist, T_{reg}-depleting, or agonist reagent.

Here, we evaluate the activity of murine and human anti-TNFR2 antibodies for cancer therapy. Further, we describe in detail the mechanism of action of a novel mouse TNFR2 antibody (Y9) that binds to the receptor outside of the TNF-binding region and is highly active in preclinical mouse models. Our evidence suggests that Fc-dependent agonism of conventional T cells is the dominant mechanism of action for its antitumor activity. Finally, we report the development and activity of corresponding human agonist TNFR2 antibodies for use in patients.

RESULTS

Characterization of novel murine anti-TNFR2 antibodies

The evaluation of TNFR2-targeted cancer therapeutics is hampered by the low degree of sequence identity in the extracellular domain between human and murine TNFR2 receptors (57.1%) and, consequently, the difficulty in finding cross-reactive antibodies. In addition, therapeutic antibodies often rely on engagement with immune cells via binding of Fc gamma receptors (FcγRs), which further complicates the direct

[1]Merrimack Pharmaceuticals, Inc., Cambridge, MA 02139, USA. [2]Histo-Scientific Research Laboratories, Mount Jackson, VA 22842, USA. [3]University of California at San Francisco, San Francisco, CA 94110, USA. [4]La Jolla Institute for Immunology, La Jolla, CA 92037, USA. [5]University of California San Diego, La Jolla, CA 92037, USA.
*These authors contributed equally to this work.
†Corresponding author. Email: ertam604@gmail.com (E.M.T.); andreas.raue@me.com (A.R.)

testing of human therapeutic antibodies in immunocompetent mouse models with incongruous FcγRs. Therefore, we sought to generate a panel of murine anti-TNFR2 antibodies for evaluation as surrogate therapeutics in syngeneic mouse tumor models. We identified antibodies that bound specifically to murine TNFR2 through rabbit immunization and panning of a human single-chain variable fragment (scFv) yeast library. None of the identified antibodies were cross-reactive to human TNFR2. Anti-murine TNFR2 antibodies were produced as mouse IgG2a proteins and epitope mapping was performed using a panel of chimeric murine/human receptor constructs, in which regions of the cysteine-rich domains (CRDs) of the murine receptor were replaced with the corresponding regions of the human receptor. We identified five novel anti-TNFR2 antibodies (Y9, M3, Y7, Y10, and H5L10) that bound unique epitopes spanning all four CRDs of the mouse receptor (Fig. 1A). The affinities of the antibodies for murine TNFR2 were measured using biolayer interferometry (BLI), and we observed the following rank order from highest to lowest affinity: Y9 (0.2 nM), Y10 (0.5 nM), H5L10 (1.0 nM), M3 (2.8 nM), and Y7 (25 nM). We calculated the sequence identity of TNFR2 to other TNFR superfamily members and found it to be 12.6% to TNFR1, 19.6% to OX-40, 21.3%

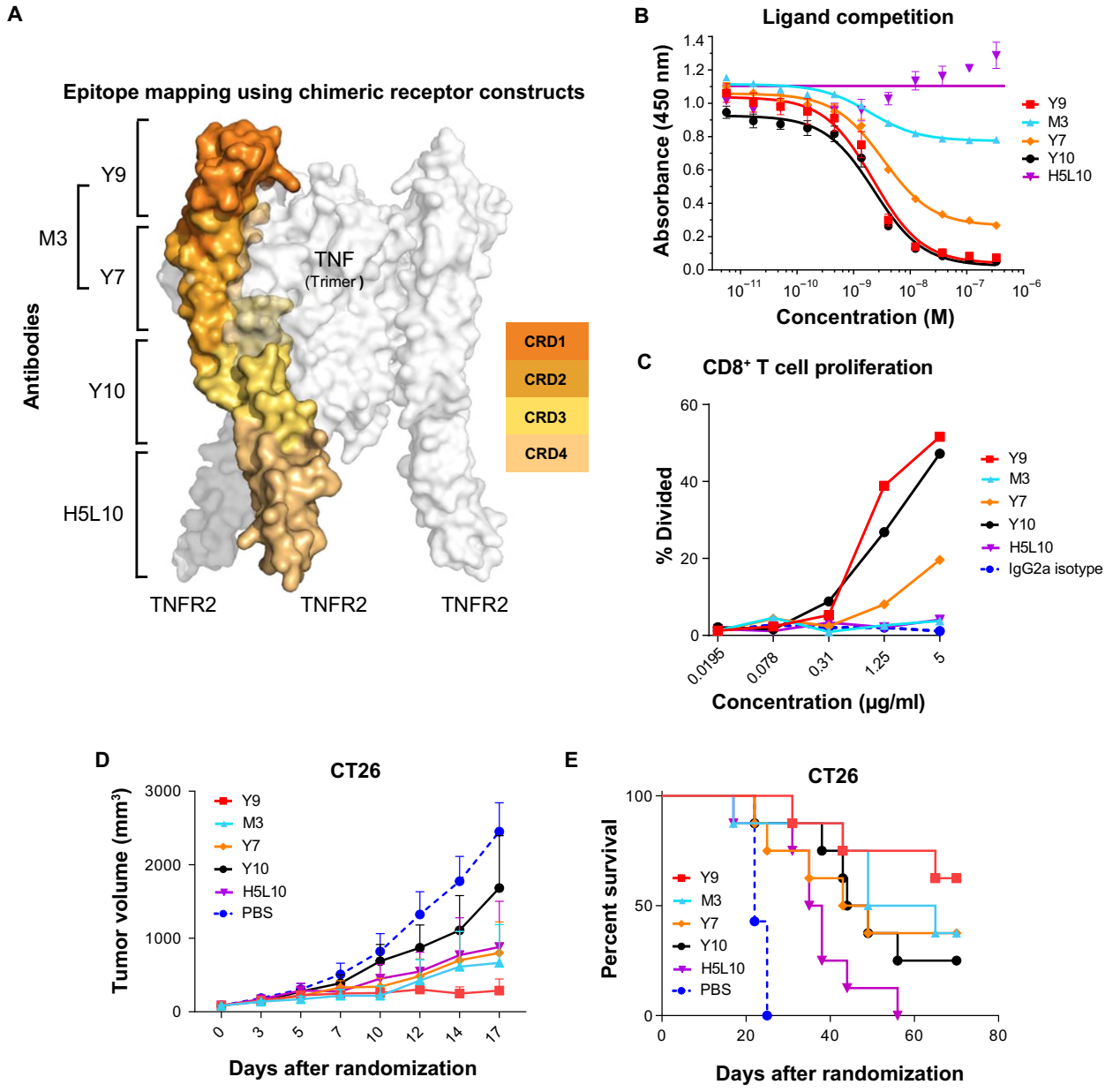

Fig. 1. Characterization of anti-mouse TNFR2 antibodies in vitro and in vivo. (**A**) The domain epitopes of antibodies are indicated on a homology model of the murine TNFR2/TNF complex. The CRDs for one TNFR2 receptor are shown in color. (**B**) TNF competition ELISA of antibodies. Data represented as a three-parameter dose-response curve fit based on mean and SD ($n = 2$). (**C**) Comparison of in vitro CD8$^+$ T cell proliferation for different anti-TNFR2 antibodies [plate-bound anti-CD3 (0.2 μg/ml) plus soluble anti-CD28 (1 μg/ml)]. Data are representative of two independent experiments. (**D**) In vivo activity in the CT26 syngeneic murine tumor model. Each antibody was injected intraperitoneally once at day 0 (9 days after tumor inoculation) at 1 mg ($n = 7$ animals per group, data displayed as mean ± SEM). (**E**) In vivo activity in the CT26 syngeneic murine tumor model at a reduced dose. Each antibody was injected intraperitoneally once at day 0 (9 days after tumor inoculation) at 300 μg ($n = 8$ animals per group).

to glucocorticoid-induced TNFR family related gene (GITR), and 22.7% to 4-1BB. We validated that the TNFR2 antibodies did not bind to GITR, 4-1BB, OX-40, and TNFR1 using enzyme-linked immunosorbent assay (ELISA) (fig. S1).

We next evaluated whether these antibodies could compete for TNF binding to TNFR2 by ELISA. Both Y7 and Y10 antibodies were able to block TNF binding (Fig. 1B), which is consistent with their epitopes overlapping with the ligand interface in CRD2 and CRD3. M3 only partially blocked TNF binding, whereas H5L10 did not block TNF binding at all; both findings are consistent with the epitope mapping. Interestingly, Y9 was observed to be a potent TNF blocker despite binding outside of the ligand interface in CRD2 and CRD3 (Fig. 1B).

We hypothesized that antibody-mediated engagement of TNFR2 could exhibit costimulatory activity on conventional T cells, similar to other members of the TNFR superfamily (*25*–*28*). To evaluate our anti-mouse TNFR2 antibodies, we stimulated naïve mouse $CD8^+$ T cells with suboptimal doses of anti-CD3 and anti-CD28 and increasing amounts of the anti-TNFR2 antibodies, and measured their proliferation using flow cytometry (Fig. 1C). Y9, followed by Y10 and Y7, induced proliferation of $CD8^+$ T cells whereas M3 and H5L10 were indistinguishable from isotype control. Supporting agonist activity, Y9 also up-regulated expression of granzyme B, CD25, and PD-1 (fig. S2A). Importantly, Y9-mediated costimulation required higher-order TNFR2 cross-linking (soluble versus plate-bound, fig. S2B). Y9 provided similar costimulation as well to conventional $CD4^+$ T cells (fig. S2C) and T_{regs} (fig. S2D) and required TCR stimulation. We further showed that Y9 mediates NFκB signaling, known to be important for effector T cell proliferation, survival, and cytokine production, in a TNFR2-overexpressing reporter cell line (fig. S2E). We also established a T_{reg} and T effector cell coculture and measured T effector cell prolifation and found that Y9 treatment did not alter the suppressive capabilities of T_{regs} in vitro (fig. S3). These data suggest that some anti-TNFR2 antibodies, exemplified by Y9, can provide costimulation to T cells.

To determine in vivo antitumor activity of our TNFR2 antibodies, we treated mice bearing established CT26 syngeneic tumors with 1 mg of each of the antibodies (Fig. 1D). Consistent with having the strongest signal in the in vitro costimulation assay, Y9 treatment provided the greatest antitumor activity in vivo. The antibodies M3 and H5L10, which did not strongly affect ligand binding or in vitro costimulation, also had activity in vivo. This suggests that competition with TNF is not required for antitumor activity of TNFR2-targeted antibodies and that the in vitro assay was not sufficiently sensitive or these antibodies have a unique mechanism of action in vivo.

To further differentiate between the novel antibodies, we treated CT26 tumor-bearing mice with a lower dose (300 μg) of each antibody and monitored the long-term antitumor response (Fig. 1E). Consistent with the previous experiment, Y9 showed the greatest activity, with more than 50% of the mice surviving more than 70 days. The Y7, Y10, and M3 antibodies also retained activity at the lower dose, with approximately 25% of the mice surviving, whereas H5L10 did not show any long-term responses at the lower dose (Fig. 1E). In summary, we identified a panel of novel anti-mouse TNFR2 antibodies where Y9 showed the greatest costimulatory activity in vitro and the strongest antitumor activity in the CT26 model in vivo.

Anti-TNFR2 antibody Y9 is active in multiple syngeneic mouse tumor models

To understand whether syngeneic tumors were broadly responsive to anti-TNFR2, we treated eight different tumor models with a single lower dose of Y9 (300 μg), and we monitored the long-term antitumor response (Fig. 2A). We found responses in five out of eight models, with four models showing mice with a complete response (CR; tumors below 60 mm^3 and continued to regress until the end of the study). To evaluate the activity of Y9 relative to treatment with anti–PD-1, we generated a murine version of the hamster anti-mouse PD-1 antibody J43 (*29*). Both antibodies were then tested in anti–PD-1–sensitive (Sa1/N) and anti–PD-1–resistant (MBT-2) syngeneic mouse models (Fig. 2B). In both models, Y9 treatment alone led to CR in all treated animals. To evaluate whether treatment with Y9 could enhance the response to anti–PD-1, we tested the treatment combination for activity in three syngeneic mouse models (Fig. 2C). In the WEHI-164 model, Y9 treatment alone was comparable to anti–PD-1, and the combination did not improve the antitumor activity. However, in the CT26 and EMT6 models, the combination of Y9 and anti–PD-1 treatment showed greater survival. We also generated a murine version of the programmed death-ligand 1 (PD-L1) antibody MPDL3280a (*30*) and obtained similar results in all three models (fig. S4). Therefore, anti-TNFR2 displays durable activity against multiple tumor types that is equivalent to and, in some cases, better than anti–PD-1 or anti–PD-L1, and anti-TNFR2 can be used in combination with anti–PD-1 or anti–PD-L1 for enhanced antitumor activity in less immunogenic tumors.

To determine whether Y9 induces immunological memory, tumor-free mice from the Y9 treatment groups were rechallenged with tumor in parallel with age-matched, tumor-naïve wild-type mice as controls (Fig. 3). Whereas all the mice in the age-matched control group grew tumors, most of the mice in the Y9 treatment groups remained tumor-free (6 of 7 mice in the CT26 model, 13 of 13 mice in the WEHI-164 model, and 4 of 5 mice in the EMT6 model). We conclude that anti-TNFR2 treatment not only results in short-term antitumor activity but can also induce long-term immune memory in multiple tumor models.

Anti-TNFR2 antibody activity requires FcγR binding

It has been shown for agonistic antibodies that target the TNF superfamily of costimulatory receptors that receptor cross-linking mediated by antibody binding to FcγR is critical for their activity (*31*), likely through allowing the formation of higher-order receptor clusters (*32*, *33*). To investigate whether the Y9 antibody requires FcγR binding for its in vivo activity, a variant of Y9 with Fc mutations D265A and N297A (Y9-DANA), which are known to abrogate binding to FcγRs, was generated (*34*, *35*). We then compared the activity of the wild-type Y9 and Y9-DANA antibodies in CT26, WEHI-164, and EMT6 tumor models (Fig. 4A). Wild-type Y9 showed the expected activity in all three models but the Y9-DANA variant lacked activity. Given that Y9-DANA blocks TNF binding comparably to wild-type Y9 (fig. S5), we therefore concluded that antagonizing the TNF/TNFR2 signaling axis is not a core mechanism of Y9.

FcγR engagement of an antibody can indicate contribution of effector functions, such as antibody-dependent cellular cytotoxicity (ADCC), opsonization or antibody-dependent cellular phagocytosis (ADCP), or enhanced agonism (*36*, *37*). To evaluate which FcγRs are the most important for activity, we tested Y9 in the CT26 model inoculated in either wild-type BALB/c mice (WT), BALB/c knockout mice that lack the inhibitory mFcγRIIb receptor (*Fcgr2b*$^{-/-}$), and BALB/c knockout mice that lack the common Fc-gamma chain (*Fcer1g*$^{-/-}$), rendering the mice deficient in expression of the activating FcγRs: mFcγRI, mFcγRIII, and mFcγRIV (*38*). The treatment control groups in the three different strains were indistinguishable but Y9 activity was significantly

reduced in both *Fcgr2b*$^{-/-}$ and *Fcer1g*$^{-/-}$ mice ($P < 0.05$; Fig. 4B). Since knockout of both activating and inhibitory FcγRs affects activity, these data suggest that enhanced agonistic activity by FcγR binding is important but does not rule out that ADCC or ADCP could also contribute to the activity of Y9 in vivo.

To further study the contribution of the different FcγRs, we investigated various IgG isotypes which have different binding affinities for FcγRs (*39*). IgG1 antibodies in human and, correspondingly, IgG2a in mouse (mIgG2a) are the dominant isotypes for mediating ADCC or ADCP because of their high affinity for activating FcγRs. In addition,

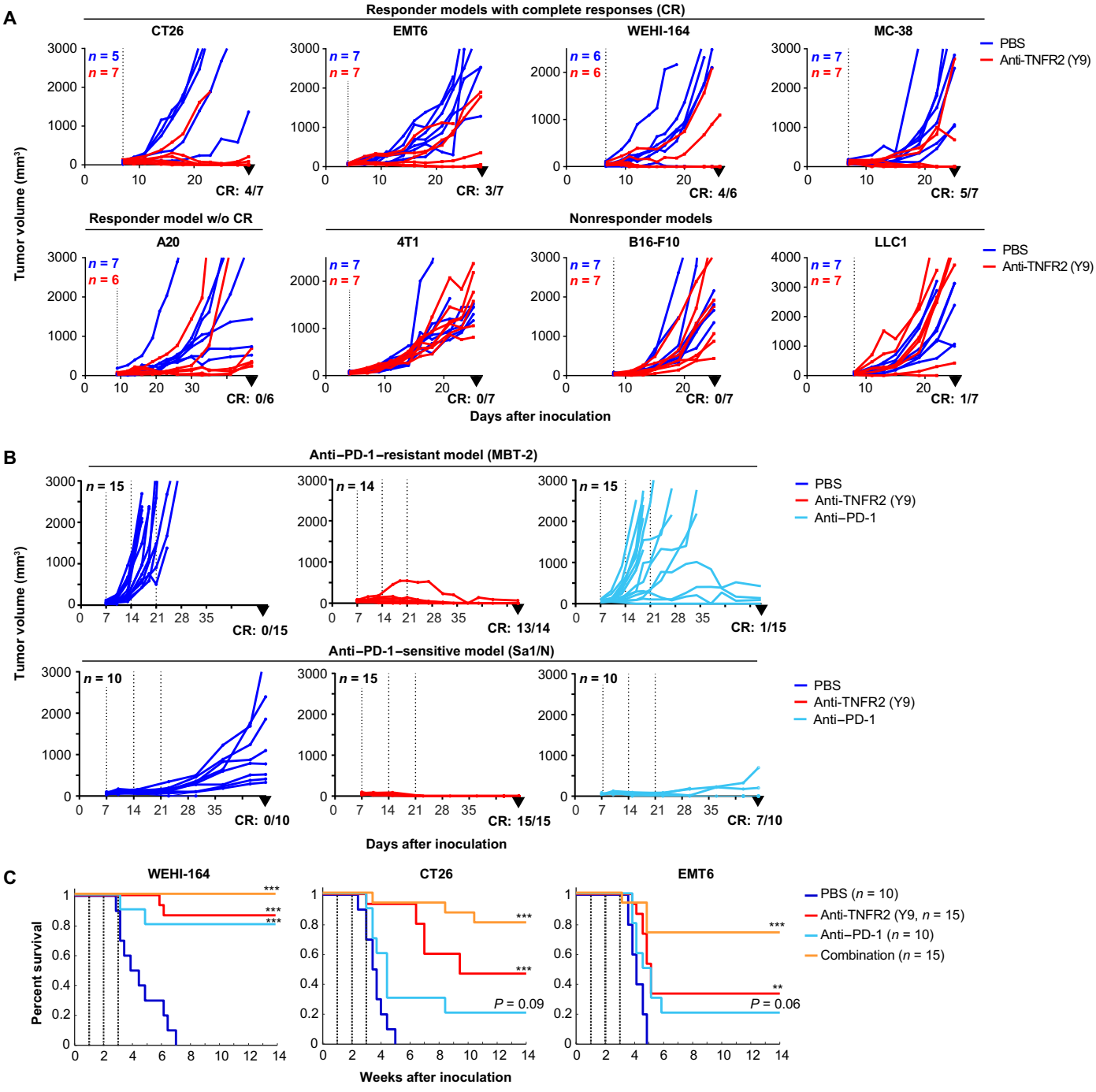

Fig. 2. In vivo activity of Y9 in syngeneic tumor models. Tumor cells were implanted and mice were randomized to treatment groups. CR, tumors below 60 mm^3 and continued to regress until the end of the study. Vertical dotted lines indicate treatment time points with 300 μg per treatment and antibody. Group sizes are indicated in the figure. (**A**) Antitumor activity of Y9 in responder and nonresponder models. Tumor growth in individual mice is shown; CR indicated for Y9 treatment groups. (**B**) Antitumor activity of Y9 in the anti–PD-1–resistant model MBT-2 and in the anti–PD-1–sensitive model Sa1/N. Tumor growth in individual mice is shown. (**C**) Survival curves for treatment with Y9 alone and in combination with anti–PD-1 in multiple murine models. Statistically significant differences from PBS are indicated. Calculated with Mantel-Cox test. $^{**}P < 0.01$, $^{***}P < 0.001$.

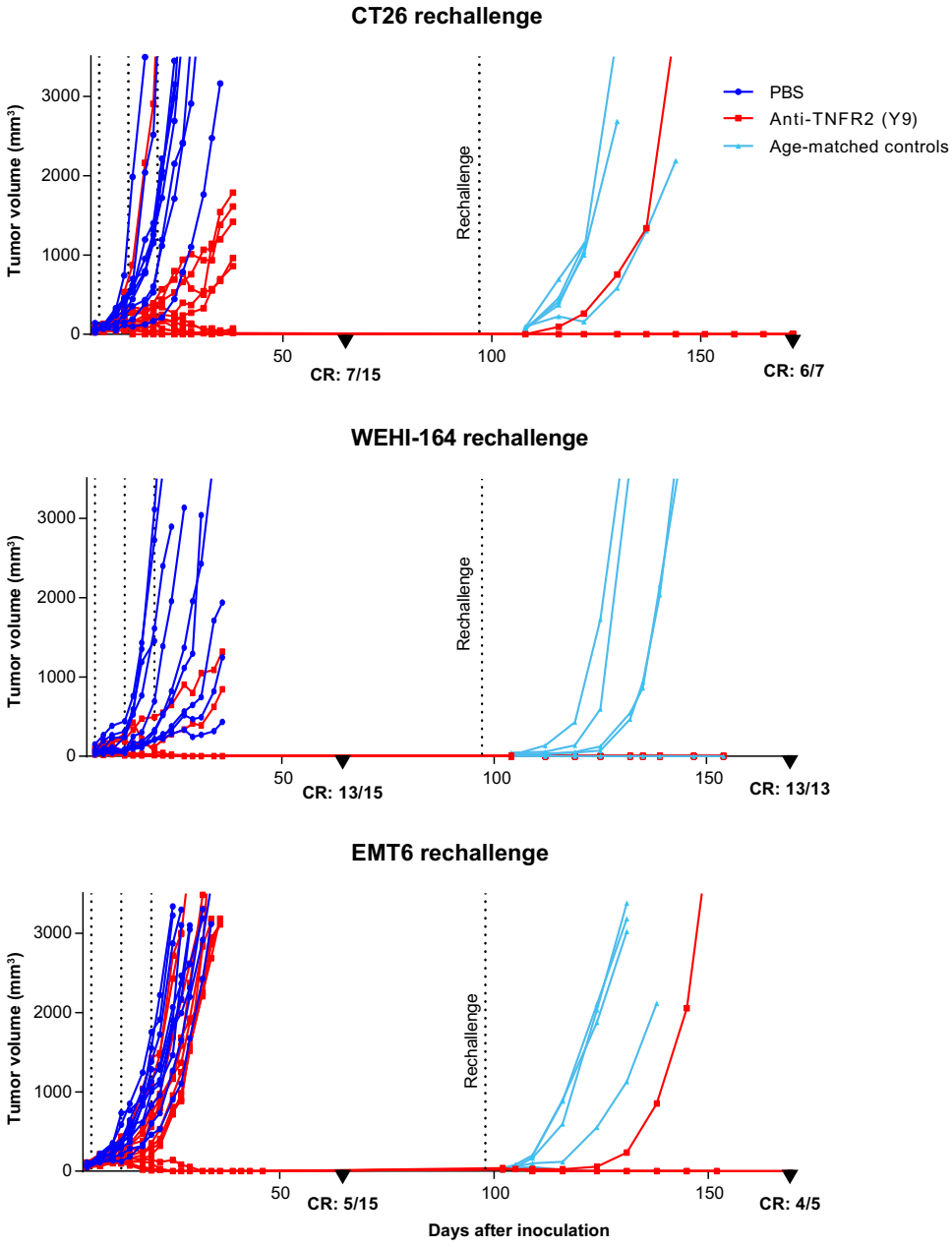

Fig. 3. Tumor rechallenge and immune memory in CT26, WEHI-164, and EMT6 models. Tumor growth in individual mice is shown (PBS, $n = 10$; Y9, $n = 15$). After initial treatment with Y9, 7 complete responder mice for the CT26 model, 13 complete responder mice for the WEHI-164 model, and 5 complete responder mice for the EMT6 model, as well as age-matched controls for each model ($n = 5$) were rechallenged with tumor cells between days 90 and 100 after inoculation. Vertical lines before rechallenge indicate days of treatment with 300 μg per antibody intraperitoneally.

mutations that increase engagement of the inhibitory FcγRIIb and thus enhance the agonistic activity have been described (*40*, *41*). We created additional Y9 variants using the following IgG isotypes and mutations in the Fc portion of the antibody: a murine IgG1 with intermediate affinity for mFcγRIIb and mFcγRIII (Y9-mIgG1), and a murine IgG2a with S267E and L328F mutations (Y9-SELF) with increased affinity for mFcγRIIb (*40*). We then compared the in vivo activity of all four Y9 variants in the CT26 and EMT6 syngeneic mouse models (Fig. 4C). We observed that the Y9-SELF and the Y9-IgG1 variant, which have a higher preference for binding the inhibitory FcγRIIb receptor, did not lose activity compared to the mIgG2a-based Y9. The Y9-DANA variant again lacked activity, as seen in other models. Collectively, these data suggest that enhanced agonistic activity mediated by FcγR clustering is the dominant contributor to the in vivo activity of the Y9 antibody.

Anti-TNFR2 treatment is mediated by CD8$^+$ T cells and NK cells, down-regulates TNFR2 on T cells, leads to CD8$^+$ T cell expansion and improved functionality, but does not deplete T$_{regs}$

We next examined the immune cell types critical for Y9 activity by depleting either CD8$^+$ T cells, CD4$^+$ T cells, or natural killer (NK) cells before inoculation with CT26 tumor cells and antibody treatment. Depletion of CD8$^+$ T cells and NK cell reduced the activity of Y9 (Fig. 5A), although the degree of dependency on these immune cell subsets varied in the WEHI-164 model (fig. S6A). In the CD4$^+$ T cell–depleted group, CT26 tumors did not establish properly and regressed spontaneously in the absence of additional treatment (Fig. 5A). We hypothesized that depletion of T$_{regs}$, as part of the broader CD4$^+$ T cell depletion, caused tumor regression in this experimental condition. However, it has been shown that the CT26 model can be established with Matrigel to circumvent this limitation (*42*). As reported, CT26 tumors were established with Matrigel and continued to grow in the CD4$^+$ T cell–depleted experimental condition (Fig. 5B). Y9 treatment remained active in the absence of CD4$^+$ T cells, indicating that neither conventional nor regulatory CD4$^+$ T cells are required for anti-TNFR2 activity in this model.

Previously, it has been suggested that TNFR2 is an oncogene (*16*) and that an anti-TNFR2 antibody directly inhibits the proliferation of TNFR2-expressing cancer cells (*21*). We also detected TNFR2 expression on mouse tumor cells (fig. S6B). To investigate whether Y9 has any direct activity on cancer cells, we generated TNFR2 knockout tumor cell lines of CT26, EMT6, and MC38 using CRISPR-Cas9 (fig. S6B) and tested Y9 activity in vivo. For all three knockout cell lines, the tumors grew at a rate that was comparable to parental cells. Moreover, Y9 remained active in all three knockout models (Fig. 5C and fig. S6C), suggesting that anti-TNFR2 primarily exerts its therapeutic activity through immune cells.

To further investigate how anti-TNFR2 therapy affects the immune compartment, we profiled tumor-infiltrating immune cells and immune cells in the tumor-draining lymph nodes (tdLN) by

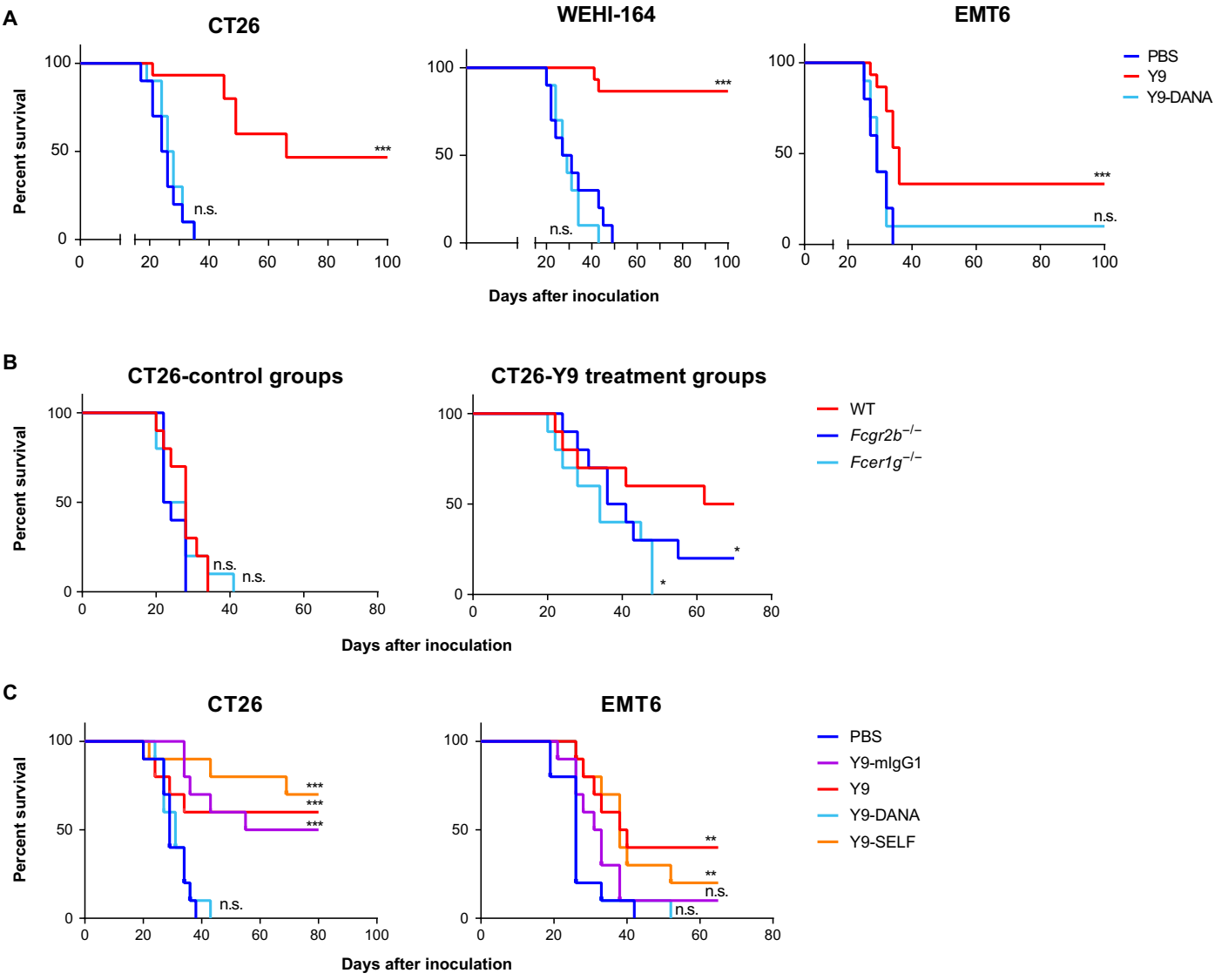

Fig. 4. Importance of FcγR binding. (**A**) Comparison of in vivo activity of Y9 with wild-type Fc (Y9) and DANA mutant Fc (Y9-DANA) shown as survival curves in three syngeneic mouse models. Antibodies were injected intraperitoneally at 300 μg on days 5, 12, and 19 after tumor inoculation. Statistically significant differences from PBS are indicated (PBS, $n = 10$; Y9, $n = 15$; Y9-DANA, $n = 10$). (**B**) In vivo activity of Y9 in CT26 syngeneic murine tumor model in BALB/c wild-type (WT), Fc receptor common γ-chain knockout (*Fcer1g*$^{-/-}$), and FcγR2b knockout (*Fcgr2b*$^{-/-}$) mouse strains. Data are shown as survival curves. Antibodies were injected intraperitoneally at 300 μg on days 8, 15, and 22 after inoculation. Statistically significant differences from WT is indicated ($n = 10$ mice per group). (**C**) Comparison of in vivo activity of Y9 with wild-type mIgG2a Fc (Y9), mIgG2a Fc with DANA mutations (Y9-DANA), wild-type mIgG1 Fc (Y9-mIgG1), and mIgG2a Fc with SELF mutations (Y9-SELF). Data are shown as survival curves for two syngeneic mouse models. Antibodies were injected intraperitoneally at 300 μg on days 8, 15, and 22 after inoculation. Data were analyzed using Mantel-Cox test. Statistically significant differences from PBS are indicated ($n = 10$ mice per group). *$P < 0.05$, **$P < 0.01$, ***$P < 0.001$. n.s., not significant.

flow cytometry after injection of Y9 in multiple syngeneic mouse models (Fig. 5, D to G). As an additional control, we included the Y9-DANA variant that lacked in vivo activity but retained TNFR2 binding and ligand-blocking properties. We observed decreased surface expression of TNFR2 on all investigated tumor-infiltrating T cell subsets 24 to 36 hours after Y9 but not Y9-DANA treatment (Fig. 5D), including conventional CD8$^+$ and CD4$^+$ T cells as well as T_{regs}. TNFR superfamily signaling brought about by receptor clustering can lead to reduced cell surface levels due to shedding and, consequently, lead to accumulation of soluble receptor in serum (*43*). Consistent with the literature, Y9 treatment caused elevated soluble TNFR2 in murine serum 4 and 24 hours after treatment with Y9 (fig. S6D), further suggesting that the antibody functioned through inducing costimulatory signaling. Moreover, 4 to 6 days after injection in mice with established CT26 tumors, Y9 treatment led to the expansion and increased functionality of tumor antigen–specific (AH1 $gp70_{423–431}$/H-2L^d) CD8$^+$ T cells in the CT26 model relative to Y9-DANA treatment (Fig. 5E and fig. S7). Y9 treatment increased the frequency of AH1-specific CD8$^+$ T cells within the total tumor-infiltrating CD8$^+$ T cell pool (Fig. 5E) and caused a notable decrease in PD-1 expression (fig. S7C). Whereas AH-1–specific CD8$^+$ T cells were functionally exhausted in Y9-DANA–treated mice, they were highly functional in Y9-treated mice, with an increased frequency of cells capable of producing interferon-γ (IFN-γ) and TNF (Fig. 5E and fig. S7D). The number of the IFN-γ–producing

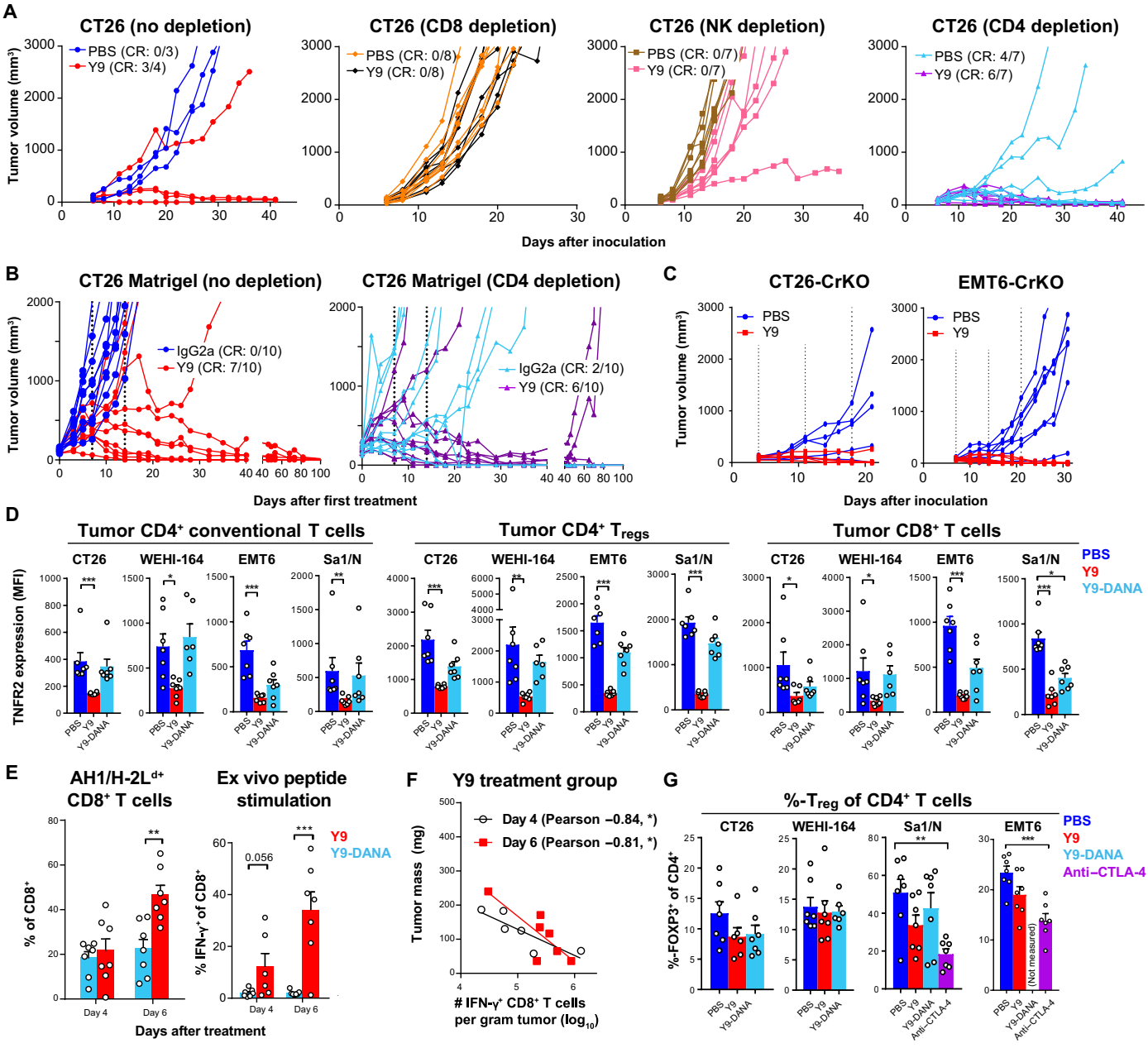

Fig. 5. Impact of treatment with Y9 on different immune cell subsets. (**A**) In vivo activity of Y9 treatment after depletion of $CD8^+$ T cells, NK cells, $CD4^+$ T cells, and no depletion control in the CT26 syngeneic murine tumor model. Once tumors were established, mice were given a single injection of 1 mg of Y9 intraperitoneally; individual mice are shown. CR, tumors below 60 mm^3 and continued to regress until the end of the study. Group sizes are indicated in the figure. (**B**) In vivo activity of Y9 treatment (300 μg × 3 weeks) after depletion of $CD4^+$ T cells and no depletion control in CT26 tumor model established with Matrigel matrix. Group sizes are indicated in the figure. Vertical dashed lines indicate days of treatment. (**C**) In vivo activity of Y9 in TNFR2 CRISPR knockout models CT26-CrKO ($n = 5$ mice per group) and EMT6-CrKO ($n = 10$ mice per group). Mice were given three weekly treatments of 300 μg of antibody intraperitoneally Individual mice are shown. (**D** to **G**) In four syngeneic murine tumor models, mice were injected intraperitoneally with 300 μg of Y9 or Y9-DANA when tumors reached 200 to 400 mm^3 (7 to 10 days after inoculation). Data were analyzed using a nonparametric Kruskal-Wallis test with a Dunn's multiple comparison test within each cell type. Data are plotted as mean ± SEM. Statistically significant differences from control are indicated. (D) TNFR2 surface expression on T cell subsets. Tumor-infiltrating immune cells were characterized 24 to 36 hours after treatment ($n = 7$ per group). (E and F) Tracking of the antitumor $CD8^+$ T cell response specific to AH1 antigen in the CT26 tumor model 4 and 6 days after treatment. Left: AH1 dextramer$^+$ CD8 T cells as a percentage of the total CD8 T cell tumor infiltrate. Right: percentage of IFN-γ^+ CD8 T cells after ex vivo peptide stimulation. Statistical comparisons were calculated using unpaired *t* tests without assuming a consistent SD. (F) Correlation of tumor mass in Y9-treated mice at day 4 or day 6 with number of IFN-γ^+ $CD8^+$ T cells per gram of tumor. Data in (E) and (F) are representative of one experiment for day 4 and two independent experiments for day 6. (G) Percentage of T_{regs} within tumoral $CD4^+$ T cells. Tumor-infiltrating immune cells were characterized 24 to 36 hours after treatment ($n = 7$ per group). Data were analyzed using ANOVA with a Dunnett's multiple comparisons posttest comparing treatment groups to control. *$P < 0.05$, **$P < 0.01$, ***$P < 0.001$.

$CD8^+$ T cells correlated with reduced tumor mass (Fig. 5F). Importantly, T_{reg} depletion, which has been reported after treatment with antibodies such as anti-GITR and anti–CTLA-4 (*44*), was not observed with anti-TNFR2 treatment across responder models (Fig. 5G and fig. S8A). In addition, Y9 did not change the $CD8^+$ T cell–to–T_{reg} ratio in either the tumor or the tdLN 24 to 36 hours after treatment, whereas an anti–CTLA-4 antibody did change this ratio in the tumor (fig. S8B). The ratio change was driven by a specific decrease in T_{regs} (Fig. 5G), as expansion of conventional $CD8^+$ and $CD4^+$ T cells was not observed for anti–CTLA-4 at this early time point. We also investigated the potential impact of Y9 treatment on cells in the myeloid compartment such as monocytes, macrophages, and neutrophils, but did not find consistent changes across different syngeneic models (fig. S9). Overall, these data suggest that costimulation of $CD8^+$ T cells is a dominant mechanism of action of Y9.

Anti-TNFR2 antibody has a favorable toxicity profile compared to anti–CTLA-4 in murine models

Given the strong antitumor immune activity, we also investigated the toxicity profile of the Y9 anti-TNFR2 antibody. We included an anti–CTLA-4 antibody with a mIgG2a-Fc as a positive control and comparator (*45*), because of its known immune-related adverse events in the clinic (*6*, *7*). We then performed a long-term exposure study in healthy 6- to 8-week-old BALB/c and C57BL/6 female mice (Fig. 6 and figs. S10 and S11), comparing weekly injections (1 mg) for both antibodies. In BALB/c mice, no difference in weight was detected across groups for the first 6 weeks of treatment; however, after the seventh dose, significant weight loss in the anti–CTLA-4 group was observed ($P < 0.001$; Fig. 6A). At the end point of the study, splenomegaly was only observed in mice treated with anti–CTLA-4 (Fig. 6B and fig. S10A). Significant increases in blood alanine aminotransferase (ALT) and aspartate aminotransferase (AST) were only observed in the anti–CTLA-4 group ($P_{ALT} < 0.001$; $P_{AST} < 0.01$; fig. S10B); however, all groups were within the normal range. To profile the effect of treatment on immune cell phenotype, we analyzed peripheral blood T cells and dendritic cells (DCs) from skin-draining lymph nodes. In mice treated with anti–CTLA-4, the frequency of acutely activated ($PD\text{-}1^+$) and proliferating ($Ki\text{-}67^+$) $CD4^+$ and $CD8^+$ T cells increased relative to isotype controls (Fig. 6, C and D, and fig. S10, C and D). In contrast, mice treated with Y9 showed no increase in T cell proliferation or acute activation markers, indicating that, unlike anti–CTLA-4, anti-TNFR2 does not cause spontaneous activation and proliferation of peripheral T cells. In addition, as previously reported (*46*, *47*), anti–CTLA-4 caused up-regulation of the costimulatory ligand CD86 (fig. S10E) on DCs, whereas Y9 did not. Importantly, Y9 did not cause histological changes in lymphoid or non-lymphoid tissues (Fig. 6E and fig. S10F), whereas anti–CTLA-4 caused widespread immune cell infiltration into tissues. Y9 caused a moderate and transient increase in serum TNF and interleukin-6 (IL-6); in contrast, anti–CTLA-4 caused chronic elevation in serum IFN-γ, TNF, IL-6, IL-5, and IL-10 (Fig. 6F and fig. S11, A and B). Similar adverse effects of the anti–CTLA-4 antibody were observed in the EMT6 tumor model, whereas mice treated with Y9 did not show any outward signs of toxicity (fig. S11C and D). In a separate study, we established that Y9 in combination with anti–PD-1 also did not induce spontaneous T cell activation, whereas anti–PD-1 in combination with anti–CTLA-4 did result in this phenomenon (fig. S12). Altogether, these data indicate that the anti-TNFR2 antibody Y9 does not lead to spontaneous immune cell activation in healthy and tumor-bearing mice.

Generation of human anti-TNFR2 antibodies modeled after the murine surrogate antibody Y9

We next sought to generate anti-human TNFR2 antibodies that would exhibit similar properties to the Y9 antibody. We developed two antibodies: Ab1, a chimeric antibody from mouse immunization, and Ab2, an affinity matured human antibody derived from human scFv phage library, the affinity of which was determined to be 700 and 200 pM, respectively (fig. S13A). As both antibodies do not bind murine TNFR2 (fig. S13B), their epitopes were mapped using human/mouse TNFR2 chimeras (fig. S13C). We observed that both Ab1 and Ab2 bind to chimera 4 and not to chimera 1, which is precisely opposite to the binding pattern of Y9, i.e., binds chimera 1 and not chimera 4 (fig. S13D), thus establishing that the Ab1 and Ab2 antibodies bind to the CRD1 region of human TNFR2. Despite binding to the same domain, Ab1 and Ab2 do not compete with one another for TNFR2 binding (fig. S13E). Consistent with the characteristics of Y9, both Ab1 and Ab2 block binding of TNF to TNFR2 with an IC_{50} (half-maximal inhibitory concentration) of 177 and 89 pM, respectively (Fig. 7A), though our data have shown that this property is not strictly required for activity. To further refine the epitopes of our human and mouse antibodies, we performed a mutational scan of surface residues in the CRD1 region for both human and mouse TNFR2. We identified positions critical for Ab1 and Y9 binding (fig. S14) but were unable to obtain data for Ab2, which did not bind yeast-displayed TNFR2. We visualized both antibody epitopes in relation to TNF binding, using the crystal structure of the human TNFR2/TNF complex (Protein Data Bank ID: 3ALQ) and a homology model of the mouse TNFR2/TNF complex (Fig. 7B). Remarkably, Ab1 and Y9 binding require structurally equivalent positions in the human (Y25, Q26, Q29, M30, and K47) and mouse (Y25, R27, K28, M31, and N47) receptor. The proximity of this epitope to human/mouse TNF suggests that Ab1 and Y9 compete with the ligand potentially steric occlusion. However, given the limited overlap between the antibody epitope and TNF interface, we do not exclude the possibility that these antibodies may also prevent ligand binding by inducing a conformational change in the receptor.

To test the agonistic potential of the anti-human TNFR2 antibodies, human T cells from pheripheral blood of healthy donors were incubated with increasing amounts of the antibodies and profiled using flow cytometry. We observed anti-TNFR2–mediated increases in proliferation, activation markers, and cytokines in both $CD4^+$ and $CD8^+$ T cells (Fig. 7, C to H). In addition, we tested the anti-human TNFR2 antibodies for antitumor activity in humanized mouse models. We engrafted human peripheral blood mononuclear cells (PBMCs) in immunodeficient NOD scid gamma (NSG) mice and then established the HT-29 colorectal adenocarcinoma cell line–derived xenograft (CDX) and observed significant antitumor activity for Ab2 ($P < 0.01$); Ab1 treatment did not have a significant effect (Fig. 8A). We also used $CD34^+$ cord blood stem cells for engraftment of a human immune system in NSG-SGM3 mice and established the MDA-MB-231 breast cancer CDX or the LG1306 NSCLC patient-derived xenograft (PDX) (Fig. 8B). In both models, we observed significant antitumor activity of Ab1 ($P < 0.05$) or Ab2 ($P < 0.01$) in combination with anti–PD-1 (nivolumab) versus anti–PD-1 alone. These data confirm that human anti-TNFR2 antibodies provide costimulation to T cells in vitro similar to the murine surrogate antibody Y9 and also provide antitumor activity in vivo comparable to, or greater than, that seen with blocking PD-1, and further enhanced activity of PD-1.

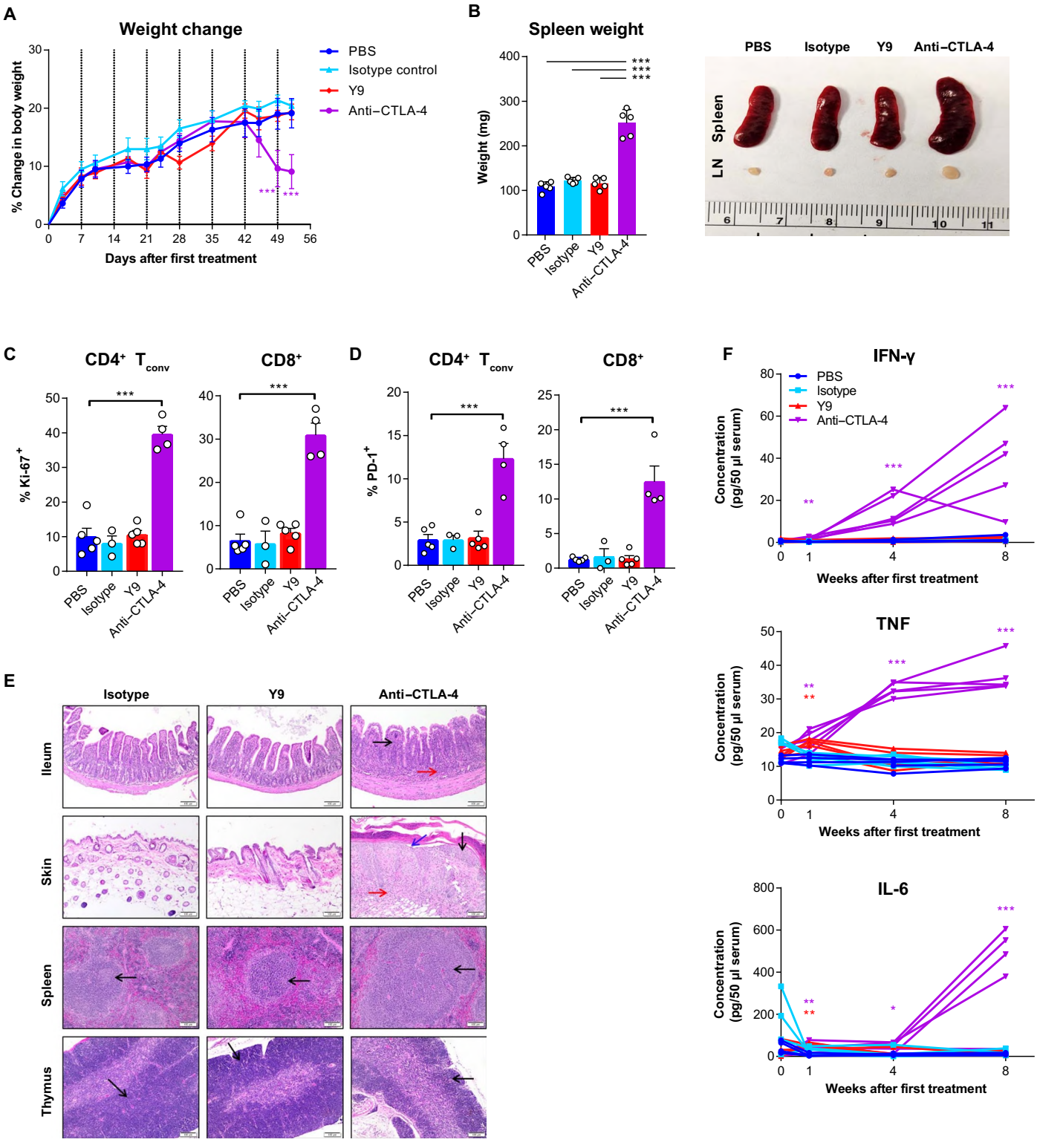

Fig. 6. Comparison of toxicity profile of long-term exposure to anti-TNFR2 or anti–CTLA-4 antibodies in BALB/c mice. Mice were treated once weekly with PBS or 1 mg of murine IgG2a isotype control, Y9, or anti–CTLA-4 for 8 weeks (n = 5 animals per group). Individual mice are shown except in (A). (**A**) Longitudinal percent change in body weight. Vertical dashed lines indicate times of treatment. (**B**) Comparison of spleen sizes and weights 48 hours after the final treatment. (**C** and **D**) Frequency of Ki-67$^+$ (C) and PD-1$^+$ (D) CD4$^+$ Foxp3^{neg} (T_{conv}) and CD8$^+$ T cells in the peripheral blood 7 days after the fourth treatment. (**E**) Representative hematoxylin and eosin (H&E) staining from various tissues in BALB/c mice treated with IgG2a isotype, Y9, or anti–CTLA-4. H&E, 100×. Indicated are inflammatory cells (red arrows), multifocal epidermal hyperplasia (black arrows), and ulceration (blue arrow). Images are representative of five animals per treatment group. (**F**) Longitudinal serum cytokines. Data were analyzed using ANOVA with a Dunnett's multiple comparisons posttest comparing treatment groups to PBS. Data are plotted as mean ± SEM. Statistical significance from PBS control is indicated. *P < 0.05, **P < 0.01, ***P < 0.001.

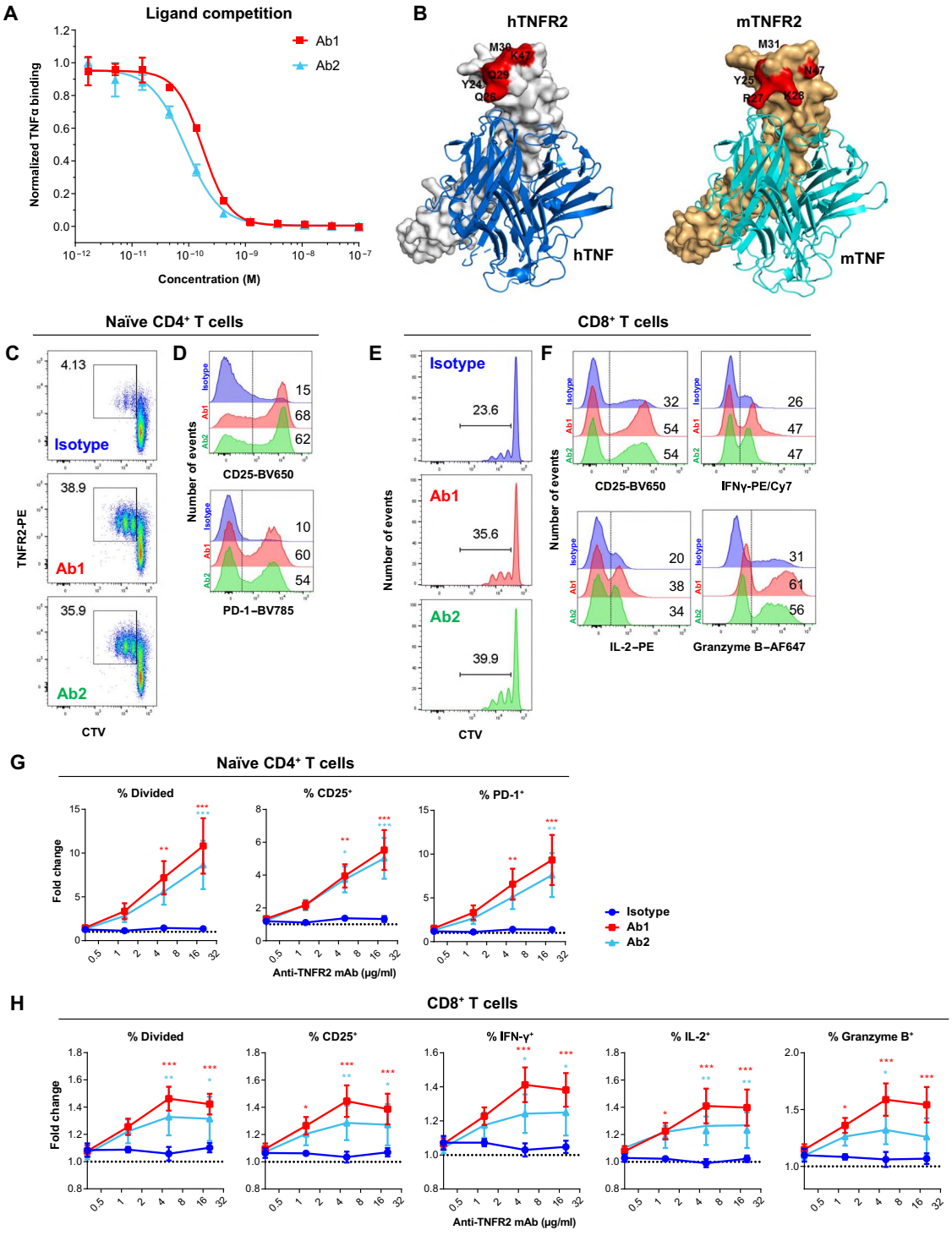

Fig. 7. Generation of anti-human TNFR2 antibodies modeled after the Y9 antibody. (**A**) Cell-based TNF competition assay of antibodies. Data represented as a three-parameter dose-response curve fit based on mean and SD from duplicate measurements. (**B**) The high-resolution epitope of anti-human (Ab1) and anti-mouse (Y9) TNFR2 antibodies is highlighted on the structure of human TNFR2 (white)/TNF (blue) and homology model of mouse TNFR2 (orange)/TNF (cyan), respectively. Residues critical for Ab1 (Y24, Q26, Q29, M30, and K47) and Y9 binding (Y25, R27, K28, M31, and N47) are highlighted (red). (**C** and **D**) In vitro costimulation of purified naïve human CD4$^+$ T cells with plate-bound anti-TNFR2 mAbs (20 μg/ml) [plate-bound anti-CD3 (5 μg/ml) plus soluble anti-CD28 (1 μg/ml)]. Representative flow plots from one healthy donor showing percent proliferation measured by CellTrace Violet (CTV) dilution (C) and induction of CD25 and PD-1 (D). Data for Ab1 are representative of three separate experiments (total of n = 11 unique donors) and Ab2 is representative of two separate experiments (total n = 8 unique donors). (**E** and **F**) In vitro costimulation of purified human CD8$^+$ T cells with plate-bound anti-TNFR2 mAbs (20 μg/ml) [plate-bound anti-CD3 (5 μg/ml)]. Representative flow plots from one healthy donor showing percent proliferation (E) and induction of CD25, IFN-γ, IL-2, and granzyme B (F). Data for Ab1 are representative of three separate experiments (total of n = 11 unique donors) and Ab2 is representative of one experiment (total n = 4 unique donors). (**G**) In vitro costimulation of naïve human CD4$^+$ T cells with titrated concentrations of plate-bound anti-TNFR2 mAbs [plate-bound anti-CD3 (5 μg/ml) plus soluble anti-CD28 (1 μg/ml)]. Graphs represent data from one experiment with four unique donors and were normalized within each donor to wells where no antibody is present. Data shown as fold-change ± SEM. Data for Ab1 are representative of three separate experiments (total of n = 11 unique donors) and Ab2 is representative of two separate experiments (total n = 8 unique donors). (**H**) In vitro costimulation of human CD8$^+$ T cells with titrated concentrations of plate-bound anti-TNFR2 mAbs [plate-bound anti-CD3 (5 μg/ml) plus soluble anti-CD28 (1 μg/ml)]. Graphs represent data from one experiment with four unique donors and were normalized within each donor to wells where no antibody is present. Data shown as fold change ± SEM. Data for Ab1 are representative of three separate experiments (total of n = 11 unique donors) and Ab2 is representative of one experiment (total n = 4 unique donors). Data were analyzed using two-way ANOVA with Dunnett's multiple comparison post tests. Statistically significant from isotype is indicated (A and B). *P < 0.05, **P < 0.01, ***P < 0.001.

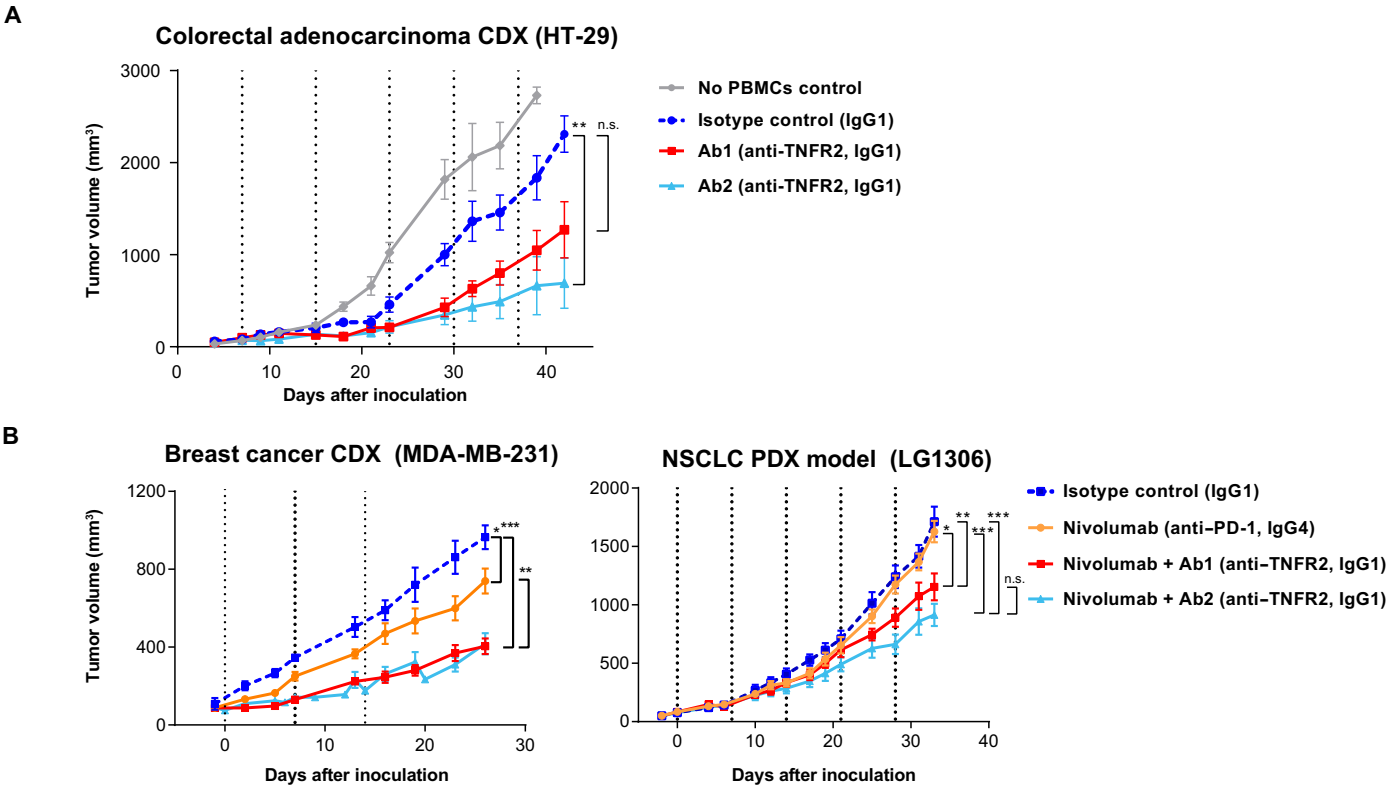

Fig. 8. Anti-human TNFR2 mAbs provide costimulation to human T cells and antitumor activity in humanized mouse models. (**A**) NSG mice were administered human PBMCs from one donor and HT-29 colorectal adenocarcinoma CDX cells on the same day. On day 7 when tumors were established (~90 mm^3), mice were given 5 × 300-μg doses of mAb (vertical dashed lines) with four to five mice per group. (**B**) NSG-SGM3 mice were engrafted with human $CD34^+$ cord blood cells. Mice that had ≥25% of total $CD45^+$ cells of human origin after 12 weeks were inoculated with MDA-MB-231 CDX or LG1306 PDX with 10 mice per group. Mice were given 300 μg doses of mAb at indicated time points (vertical dashed lines). Statistically significant from isotype is indicated. *P < 0.05, **P < 0.01, ***P < 0.001.

DISCUSSION

TNFR2 engagement affects multiple T cell types. TNF/TNFR2 can provide costimulation to antitumor T cells (*26*), but more recent research has focused on the role of TNFR2 in T_{reg} development and its ability to stabilize the T_{reg} inhibitory program (*19*, *20*). Correspondingly, reports have demonstrated the utility of anti-TNFR2 agonistic antibodies to boost effector T cell activity (*15*) or, oppositely, antagonistic antibodies that block TNF/TNFR2 signaling to destabilize inhibitory T_{regs} (*18*, *21*, *23*). In these reports, studies using anti-TNFR2 antibodies in murine syngeneic tumor models have shown at best moderate effects on tumor growth, although it was unclear whether this was a biological limitation of TNFR2 as a therapeutic target or in the design of anti-TNFR2 antibodies. Moreover, antibodies used in these studies often consisted of a non-murine Fc and did not compare the effects of different epitopes and isotypes (*15*, *23*). To address these prior limitations, we generated an extensive panel of anti-mouse TNFR2 antibodies against multiple epitopes and produced them all as mouse IgG2a for evaluation in vivo. By utilizing antibodies with the optimal Fc (species and isotype), we found that targeting TNFR2 leads to robust antitumor activity across multiple mouse models. The Y9 antibody, a TNF-competitive antibody that binds to the CRD1 region and has agonistic activity in all studied T cell subsets in vitro, displayed the greatest antitumor activity in vivo. Interestingly, agonistic antibodies binding the equivalent region in other TNFR family members, 4-1BB and CD40, are also the most active (*48*, *49*).

Consistent with data for antibodies that target similar costimulatory TNFR family members, 4-1BB, OX40, CD40, GITR, and CD27, as reviewed by Mayes *et al.* (*9*), our data indicate that the mechanism of antitumor action for the mouse antibody, Y9, is TNFR2 agonism. Supporting evidences are as follows: (i) expansion of T cells in vitro and in vivo, (ii) dependence on Fc/FcγR interaction in vivo, (iii) membrane TNFR2 down-regulation and shedding in vivo, (iv) lack of T_{reg} depletion within the tumor in vivo, (v) increased functionality of tumor antigen–specific $CD8^+$ T cells in vivo, and (vi) a correlation of $CD8^+$ T cell functionality with reduced tumor size.

Although TNFR2 is part of a larger family of costimulatory receptors that are being investigated for therapy of cancer, targeting TNFR2 may offer some differences. Presently, we show that Y9 activates both $CD8^+$ and $CD4^+$ T cells in vitro, and that Y9 loses activity in the CT26 model when these cell types are depleted. In addition, NK cells were also implicated in the activity of Y9 in vivo. Targeting TNFR2 also did not lead to considerable depletion of T_{regs}, as observed for other antibodies targeting T cell surface receptors (*44*).

Besides T cell surface receptors, it is known that myeloid cells can express TNFR2 (*50*). Our study here only provides limited insight into whether activating TNFR2 on these cell types could be beneficial. Further, our detailed investigation of Y9 does not rule out that other anti-TNFR2 antibodies might also have antitumor activity and could have different mechanisms of action, including potentially Fc-independent mechanisms. Finally, Y9 had limited effectiveness alone in poorly immunogenic

syngeneic tumor models, similar to PD-1 blockade or agonists of other TNFR family proteins. These negative data are important for the future development of biomarker strategies and the development of potential novel combination therapies, as well as for refining our understanding of the importance of the balance of activating versus inhibitory FcγRs.

Despite the broad activity, we did not see any significant toxicity after chronic treatment with anti-TNFR2, compared to an anti–CTLA-4 antibody. This is advantageous for combining with established checkpoint inhibitors, where the promise of an active and tolerable regimen remains challenging (*6*, *7*). The anti–CTLA-4 antibody, ipilimumab, has been widely studied in combination with anti–PD-1 antibodies in NSCLC and melanoma, but only at the expense of heightened immune-related adverse events, primarily driven by ipilimumab (*6*, *7*). Indeed, we observed that the combination of an anti-TNFR2 antibody with PD-1 or PD-L1 blockade further improved antitumor activity, but unlike mice treated with an anti–CTLA-4 mAb, we did not observe evidence of significant immune-related toxicities. This suggests that the combination of an agonistic anti-TNFR2 antibody with anti–PD-1 or anti–PD-L1 antibodies could result in a greater therapeutic index than the combination of anti–PD-1 with anti–CTLA-4.

We consider the preclinical data of Y9 very encouraging, justifying the clinical development of human anti-TNFR2 antibodies. The human antibodies presented here should be highly translatable given the large overlap in their corresponding epitopes especially between Ab1 and Y9. While confirmation of the Ab2 epitope is currently under investigation, we have observed significant correlation in activity between Y9 and both human antibodies in ex vivo T cell stimulation assays and in preclinical tumor models. In conclusion, we continue to advance our human antibodies toward the clinic, as we believe that agonism of TNFR2 is a compelling therapeutic strategy for engagement of the immune system in the treatment of cancer.

MATERIALS AND METHODS

Study design

The research objective was to investigate antitumor activity and mechanism of action of targeting TNFR2 with mAbs using mouse surrogates, and the development of human antibodies that were modeled after the most active murine surrogate antibody. Research subjects were animals and blood from healthy human donors. Sample size was determined before the study as per Institutional Animal Care and Use Committee (IACUC) guidelines. For animal studies, tumor volume data were recorded until tumor sizes reached maximum size as defined by IACUC guidelines. Mice were randomized to treatment groups after tumor establishment. No data were excluded, except for 2 of 5 samples in Fig. 5C in the isotype treatment group because not enough blood was available. No outliers were excluded. To ensure reproducibility, experiments were repeated independently, as described in the figures and legends. When the tumors reached an average size of 50 to 100 mm^3, mice were randomized into treatment groups to achieve comparable distribution of starting tumor volumes per condition. Studies were not blinded. Where possible, studies have been repeated by independent personnel. Primary data are reported in data file S1.

Anti-mouse TNFR2 antibodies

Anti-mouse TNFR2 antibodies were derived from selections of both human and rabbit antibody yeast libraries. The human scFv library has been described previously (*51*). The rabbit scFv library was constructed as follows. Messenger RNA was isolated from the spleens of rabbits immunized with murine TNFR2. Rabbit immunization was performed at Genscript. Briefly, two rabbits were injected subcutaneously with 0.5 mg of mTNFR2-His emulsified in complete Freund's adjuvant. Animals were then boosted with 0.25 mg of antigen emulsified in incomplete Freund's adjuvant at 2, 4, and 6 weeks. Animals were bled and euthanized at 8 weeks. Rabbit VH and VL regions were amplified by RT-PCR and converted into scFv format, and the yeast library was created using methods described previously (*51*). Both human and rabbit scFv libraries were panned against mTNFR2-Fc (300 nM) for two rounds before switching to mTNFR-His (50 to 200 nM) for subsequent rounds. High-affinity binders were sequenced after four to six rounds of fluorescence-activated cell sorting (FACS). The VH and VL regions of rabbit (Y7, Y9, Y10, and H5L10; table S2) and human (M3) scFvs were synthesized as murine IgG2a heavy and kappa light chain, respectively. Murine chimeric antibodies were expressed using the ExpiCHO expression system (Thermo Fisher Scientific) and purified using MabSelect resin (GE Healthcare).

Mice

We purchased 6- to 8-week-old female BALB/c (BALB/cAnNCrl), C57B6/J (C57B6NCrl), A/J (A/JCr), and C3H (C3H/HeNCrl) mice from Charles River Laboratories. We purchased 6- to 8-week-old *Fcer1g*$^{-/-}$ [FcRγ; C.129P2(B6)-Fcer1g^{tm1Rav}N12] and FcγRIIb$^{-/-}$ [C.129S4(B6)-*Fcgr2b*^{tm1TtK}/cAnNTac N12] mice on the BALB/c background, as well as wild-type BALB/c controls, from Taconic. NSG (NOD.Cg-*Prkdc*^{scid} *IL2rg*^{tm1Wjl}/SzJ) and NSG-SGM3 [NOD.Cg-*Prkdc*^{scid} *IL2rg*^{tm1Wjl} Tg (CMV-IL3,CSF2,KITLF)1Eac/MloySzJ] mice were purchased from the Jackson Laboratory. All mice were housed under specific pathogen–free conditions in cages of up to five animals and received special rodent diet (Teklad). Studies were approved by Merrimack's IACUC. IACUC guidelines on the ethical use and care of animals were followed.

Cell lines

The following cell lines were obtained from the American Type Culture Collection (ATCC) and maintained in RPMI 1640 (Gibco, with L-glutamine included) supplemented with 10% fetal bovine serum (FBS) (Gibco), penicillin (100 U/ml), and streptomycin (100 μg/ml) (Gibco, 100× pen/strep solution): CT26 (H-2^d) colorectal carcinoma (CRL-2638), EMT6 (H-2^d) mammary carcinoma (CRL-2755), WEHI-164 (H-2^d) fibrosarcoma (CRL-1751), A20 (H-2^d) B lymphocyte sarcoma (TIB-208), 4 T1 (CRL-2539) mammary carcinoma, and B16-F10 (H-2^b) melanoma (CRL-6475). The MC38 (H-2^b) colon adenocarcinoma cell line was obtained from the National Cancer Institute (NCI) and maintained in supplemented RPMI 1640. The Sa1/N (H-2^a) fibrosarcoma cell line (ATCC, CRL-2544) was maintained in Eagle's minimum essential medium (ATCC, with L-glutamine included) supplemented with 10% FBS and pen/strep. The LLC1 (H-2^b) Lewis lung carcinoma (ATCC, CRL-1642) was maintained in Dulbecco's modified Eagle's medium (Gibco, with L-glutamine included) supplemented with 10% FBS and pen/strep. The MBT-2 (H-2^k) murine bladder cancer cell line was purchased from the Japanese Collection of Research Bioresources (JCRB) and maintained in Iscove's modified Dulbecco's medium (Gibco, with L-glutamine and 25 mM Hepes included) supplemented with 10% FBS and pen/strep. The LG1306 NSCLC human PDX model was purchased from the Jackson Laboratory and passaged continuously in NSG mice. Human MDA-MB-231 (HTB-26) breast cancer CDX and HT-29 (HTB-38) colon adenocarcinoma CDX were purchased from ATCC and maintained in supplemented RPMI 1640. All cells were tested for mycoplasma by the

supplier or in-house (MycoAlert Mycoplasma Detection Kit, Lonza) and confirmed negative.

In vivo tumor models

All tumor cells were injected subcutaneously in 100 to 200 μl of phosphate-buffered saline (PBS) into the right flank of mice that had typically been shaved the previous day. Unless otherwise stated, the following cell numbers and mouse strains were used for inoculation: 1×10^6 MBT-2 (C3H), 5×10^6 Sa1/N (A/J), and 3×10^5 for CT26 (BALB/c), EMT6 (BALB/c), WEHI-164 (BALB/c), A20 (BALB/c), 4 T1 (BALB/c), LLC1 (BALB/c), MC38 (C57BL/6), and B16-F10 (C57BL/6). Ten to fifteen mice per treatment group were used for antitumor activity studies and 7 to 10 mice were used for pharmacodynamic studies. Tumor growth was monitored using electronic calipers, and volumes were calculated according to the following formula: $\pi/6 \times (\text{length} \times \text{width}^2)$. When the tumors reached an average size of 50 to 100 mm^3, mice were randomized into treatment groups to achieve comparable distribution of starting tumor volumes per condition. Antibody (300 μg) was injected intraperitoneally as indicated once weekly for 3 weeks in a total volume of 200 μl. Mice reached endpoint and were euthanized in antitumor activity studies when tumors reached 2000 mm^3. CR was defined as tumors below 60 mm^3 and continued to regress until the end of the study. The dose of 300 μg was selected based on pilot dose-finding studies in three tumor models (CT26, EMT6, and WEHI-164). As treatment with isotype control does not lead to CRs and antitumor activity in these models, we decided to use PBS as the control group for antitumor activity studies.

Chronic exposure study in mice

We performed a chronic exposure study in non–tumor-bearing BALB/c and C57BL/6 mice. Mice (five mice per treatment group) were injected intraperitoneally with PBS or 1 mg of murine IgG2a isotype control, anti-TNFR2 (Y9), or anti–CTLA-4 once per week in 200 μl of PBS for a total of eight injections. The anti–CTLA-4 antibody used was clone 9D9 expressed as a murine IgG2a isotype. Mouse weight was measured twice per week, and the physical condition of the mice was tracked throughout the study. Saphenous blood from all groups was collected once per week immediately before treatment, and one pretreatment bleed was performed to establish a baseline. All mice were euthanized 48 hours after the final (8th) weekly treatment, whereby spleens and skin draining LNs were harvested and weighed, and blood was collected via cardiac puncture. Liver enzymes in the blood were evaluated using the Catalyst Dx Chemistry Analyzer (IDEXX). Briefly, blood samples collected by cardiac puncture were transferred into lithium heparin whole blood separators (IDEXX). Blood ALT and AST were analyzed using the NSAID 6 CLIP (IDEXX). Tissues were harvested and placed into 10% neutral buffered formalin (Avantik Biogroup) for 24 hours and then washed and placed into 70% ethanol (Avantik Biogroup). Tissues were paraffin-embedded, and hematoxylin and eosin–stained sections were examined by a veterinary pathologist. Serum cytokine and chemokines were analyzed using the murine Proinflammatory Panel 1 V-plex kit (Meso Scale Discovery) following the manufacturer's instructions.

Anti-human TNFR2 antibodies

Ab1 was derived from hybridoma generation. Briefly, four mice were each immunized with 100 μg of human TNFR2-His, and booster injections were given at days 14, 28, 42, and 56. Hybridoma fusions from splenocytes were performed at day 60 and plated onto 96-well plates. Following 10 to 14 days of culture, hybridomas that were screened positive against antigen by ELISA were subcloned by limiting dilution. Expanded subclones were evaluated for TNFR2 positivity before variable domain sequencing. Mouse VH and VK sequences were synthesized as chimeric human IgG1 and kappa antibodies (ATUM) and produced in ExpiCHO cells (Thermo Fisher Scientific) and purified using MabSelect resin (GE Healthcare). Ab2 was derived from a human single-chain Fv phage library consisting of natural diversity in HV3–23/KV1–33 pairings (2e9 members) panned against human TNFR2-Fc for two rounds and chimera 4 for the final round. Dominant clones were produced as soluble scFvs for affinity measurements. For affinity maturation, an error-prone PCR was used to generate a yeast mutant scFv library. In addition, a focused mutagenesis library in which positions in CDRL1 (24 to 34) and CDRL2 (50 to 56) were randomized using NNS and VNS codons was also generated as a yeast scFv library. Both libraries were individually panned against human TNFR2-Fc for two to four rounds. High-affinity binders were isolated by FACS and produced as human IgG1 antibodies for subsequent evaluation. Ab2 contains mutations from both random and focused mutagenesis approach.

Humanized mouse models

Two different methods of humanization were used. In one method, human cord blood $CD34^+$ frozen cells from mixed donors were purchased from STEMCELL Technologies and engrafted intravenously into NSG-SGM3 mice (2×10^4 cells per mouse). This method results in more complete engraftment of human immune cells, including myeloid cells. Humanization was determined after 12 weeks by flow cytometry on peripheral blood; mice with ≥25% of total $CD45^+$ cells of human origin were considered humanized. These animals were inoculated with 5×10^6 LG1306 or MDA-MB-231 cells subcutaneously on the right flank. Once tumors had reached ~75 mm^3, mice were treated intraperitoneally 5× (for LG1306) or 3× (for MDA-MB-231) weekly with 300 μg of IgG1 isotype control, 300 μg of nivolumab, 300 μg of nivolumab +300 μg Ab1, or 300 μg of nivolumab +300 μg Ab2. In the second method, 1×10^7 PBMCs were administered to NSG mice intravenously (a control group did not receive PBMCs), and on the same day, mice were inoculated with 3.5×10^6 HT-29 cells subcutaneously on the right flank. In this model, only human T cells persist in the recipient mouse long term. One week later, when the tumors had reached ~90 mm^3, mice were treated intraperitoneally with 300 μg of IgG1 isotype control, 300 μg of Ab1, or 300 μg of Ab2; dosing was repeated for a total of five weekly doses.

Statistical analysis

Statistical analysis was performed as described using the GraphPad Prism 7.05 software (GraphPad Software, Inc.). For multiple comparison test, Kruskal-Wallis non-parametric test with Dunn's multiple comparison posttest was used. Comparisons were made between control and treatment groups. For survival curves, two groups were compared using the log rank test. Statistical significance is indicated as $^*P < 0.05$, $^{**}P < 0.01$, $^{***}P < 0.001$, and $^{****}P < 0.0001$. Population statistics are displayed as mean and SEM or SD, as indicated.

SUPPLEMENTARY MATERIALS

stm.sciencemag.org/cgi/content/full/11/512/eaax0720/DC1

Materials and Methods

Fig. S1. Cross-reactivity test of murine TNFR2 antibodies to other TNF superfamily receptors.

Fig. S2. Enhanced proliferation and activation of T cells mediated by higher-order TNFR2 cross-linking for Y9 costimulation in vitro.

Fig. S3. In vitro T_{reg} suppression assay.
Fig. S4. In vivo activity of Y9 and anti–PD-L1 combination.
Fig. S5. Ligand blocking of Y9-DANA.
Fig. S6. Impact of treatment with Y9 on different immune cell subsets.
Fig. S7. Ex vivo analysis of tumor-specific $CD8^+$ T cell responses.
Fig. S8. Impact of treatment with Y9 on frequency changes in the T cell compartment.
Fig. S9. Characterization of the tumor-associated myeloid compartment after anti-TNFR2 treatment.
Fig. S10. Additional data for toxicity profile of long-term exposure to anti-TNFR2 or anti–CTLA-4 antibodies in BALB/c and C57BL/6 mice.
Fig. S11. Serum cytokine data for toxicity profile of long-term exposure to anti-TNFR2 or anti–CTLA-4 antibodies in BALB/c and C57BL/6 mice and toxicity study in EMT6 tumor-bearing mice.
Fig. S12. Repeat toxicity study with anti–PD-1 combinations.
Fig. S13. TNFR2 receptor constructs used for epitope mapping and binding studies.
Fig. S14. High-resolution epitope mapping of human and mouse anti-TNFR2 antibodies.
Fig. S15. Gating strategy of mouse T cells in the tdLN and tumor.
Table S1. Description of chimeric TNFR2 constructs.
Table S2. Sequences of murine TNFR2 antibodies.
Table S3. Murine T cell flow cytometry antibodies.
Table S4. Human T cell flow cytometry antibodies.
Data file S1. Primary data.
References (*52*, *53*)

REFERENCES AND NOTES

1. S. L. Topalian, F. S. Hodi, J. R. Brahmer, S. N. Gettinger, D. C. Smith, D. F. McDermott, J. D. Powderly, R. D. Carvajal, J. A. Sosman, M. B. Atkins, P. D. Leming, D. R. Spigel, S. J. Antonia, L. Horn, C. G. Drake, D. M. Pardoll, L. Chen, W. H. Sharfman, R. A. Anders, J. M. Taube, T. L. McMiller, H. Xu, A. J. Korman, M. Jure-Kunkel, S. Agrawal, D. McDonald, G. D. Kollia, A. Gupta, J. M. Wigginton, M. Sznol, Safety, activity, and immune correlates of anti–PD-1 antibody in cancer. *N. Engl. J. Med.* **366**, 2443–2454 (2012).
2. J. D. Wolchok, V. Chiarion-Sileni, R. Gonzalez, P. Rutkowski, J.-J. Grob, C. L. Cowey, C. D. Lao, J. Wagstaff, D. Schadendorf, P. F. Ferrucci, M. Smylie, R. Dummer, A. Hill, D. Hogg, J. Haanen, M. S. Carlino, O. Bechter, M. Maio, I. Marquez-Rodas, M. Guidoboni, G. McArthur, C. Lebbé, P. A. Ascierto, G. V. Long, J. Cebon, J. Sosman, M. A. Postow, M. K. Callahan, D. Walker, L. Rollin, R. Bhore, F. S. Hodi, J. Larkin, Overall survival with combined nivolumab and ipilimumab in advanced melanoma. *N. Engl. J. Med.* **377**, 1345–1356 (2017).
3. C. Grigg, N. A. Rizvi, PD-L1 biomarker testing for non-small cell lung cancer: Truth or fiction? *J. Immunother. Cancer* **4**, 48 (2016).
4. A. Swaika, W. A. Hammond, R. W. Joseph, Current state of anti-PD-L1 and anti-PD-1 agents in cancer therapy. *Mol. Immunol.* **67**, 4–17 (2015).
5. R. Zappasodi, T. Merghoub, J. D. Wolchok, Emerging concepts for immune checkpoint blockade-based combination therapies. *Cancer Cell* **33**, 581–598 (2018).
6. L. Paz-Ares, A. Luft, D. Vicente, A. Tafreshi, M. Gümüş, J. Mazières, B. Hermes, F. Çay Şenler, T. Csőszi, A. Fülöp, J. Rodríguez-Cid, J. Wilson, S. Sugawara, T. Kato, K. H. Lee, Y. Cheng, S. Novello, B. Halmos, X. Li, G. M. Lubiniecki, B. Piperdi, D. M. Kowalski; KEYNOTE-407 Investigators, Pembrolizumab plus chemotherapy for squamous non–small-cell lung cancer. *N. Engl. J. Med.* **379**, 2040–2051 (2018).
7. J. S. Weber, M. Postow, C. D. Lao, D. Schadendorf, Management of adverse events following treatment with anti-programmed death-1 agents. *Oncologist* **21**, 1230–1240 (2016).
8. J. Medler, H. Wajant, Tumor necrosis factor receptor-2 (TNFR2): An overview of an emerging drug target. *Expert Opin. Ther. Targets* **23**, 295–307 (2019).
9. P. A. Mayes, K. W. Hance, A. Hoos, The promise and challenges of immune agonist antibody development in cancer. *Nat. Rev. Drug Discov.* **17**, 509–527 (2018).
10. M. Grell, E. Douni, H. Wajant, M. Löhden, M. Clauss, B. Maxeiner, S. Georgopoulos, W. Lesslauer, G. Kollias, K. Pfizenmaier, P. Scheurich, The transmembrane form of tumor necrosis factor is the prime activating ligand of the 80 kDa tumor necrosis factor receptor. *Cell* **83**, 793–802 (1995).
11. Y. Mukai, T. Nakamura, M. Yoshikawa, Y. Yoshioka, S.-i. Tsunoda, S. Nakagawa, Y. Yamagata, Y. Tsutsumi, Solution of the structure of the TNF-TNFR2 complex. *Sci. Signal.* **3**, ra83 (2010).
12. G. Sabio, R. J. Davis, TNF and MAP kinase signalling pathways. *Semin. Immunol.* **26**, 237–245 (2014).
13. X. Chen, R. Hamano, J. J. Subleski, A. A. Hurwitz, O. M. Z. Howard, J. J. Oppenheim, Expression of costimulatory TNFR2 induces resistance of $CD4^+$ $FoxP3^-$ conventional T cells to suppression by $CD4^+$ $FoxP3^+$ regulatory T cells. *J. Immunol.* **185**, 174–182 (2010).
14. X. Chen, J. J. Subleski, H. Kopf, O. M. Z. Howard, D. N. Männel, J. J. Oppenheim, Cutting edge: Expression of TNFR2 defines a maximally suppressive subset of mouse $CD4^+CD25^+FoxP3^+$ T regulatory cells: Applicability to tumor-infiltrating T regulatory cells. *J. Immunol.* **180**, 6467–6471 (2008).
15. G. S. Williams, B. Mistry, S. Guillard, J. C. Ulrichsen, A. M. Sandercock, J. Wang, A. González-Muñoz, J. Parmentier, C. Black, J. Soden, J. Freeth, J. Jovanović, R. Leyland, R. S. Al-Lamki, A. J. Leishman, S. J. Rust, R. Stewart, L. Jermutus, J. R. Bradley, V. Bedian, V. Valge-Archer, R. Minter, R. W. Wilkinson, Phenotypic screening reveals TNFR2 as a promising target for cancer immunotherapy. *Oncotarget* **7**, 68278–68291 (2016).
16. T. Zhao, H. Li, Z. Liu, Tumor necrosis factor receptor 2 promotes growth of colorectal cancer via the PI3K/AKT signaling pathway. *Oncol. Lett.* **13**, 342–346 (2017).
17. H. Torrey, J. Butterworth, T. Mera, Y. Okubo, L. Wang, D. Baum, A. Defusco, S. Plager, S. Warden, D. Huang, E. Vanamee, R. Foster, D. L. Faustman, Targeting TNFR2 with antagonistic antibodies inhibits proliferation of ovarian cancer cells and tumor-associated T_{regs}. *Sci. Signal.* **10**, eaaf8608 (2017).
18. H. Torrey, M. Khodadoust, L. Tran, D. Baum, A. Defusco, Y. H. Kim, D. L. Faustman, Targeted killing of TNFR2-expressing tumor cells and T_{regs} by TNFR2 antagonistic antibodies in advanced Sézary syndrome. *Leukemia* **33**, 1206–1218 (2019).
19. K.-S. N. Atretkhany, I. A. Mufazalov, J. Dunst, A. Kuchmiy, V. S. Gogoleva, D. Andruszewski, M. S. Drutskaya, D. L. Faustman, M. Schwabenland, M. Prinz, A. A. Kruglov, A. Waisman, S. A. Nedospasov, Intrinsic TNFR2 signaling in T regulatory cells provides protection in CNS autoimmunity. *Proc. Natl. Acad. Sci. U.S.A.* **115**, 13051–13056 (2018).
20. M. Chopra, M. Biehl, T. Steinfatt, A. Brandl, J. Kums, J. Amich, M. Vaeth, J. Kuen, R. Holtappels, J. Podlech, A. Mottok, S. Kraus, A.-L. Jordán-Garrote, C. A. Bäuerlein, C. Brede, E. Ribechini, A. Fick, A. Seher, J. Polz, K. J. Ottmüller, J. Baker, H. Nishikii, M. Ritz, K. Mattenheimer, S. Schwinn, T. Winter, V. Schäfer, S. Krappmann, H. Einsele, T. D. Müller, M. J. Reddehase, M. B. Lutz, D. N. Männel, F. Berberich-Siebelt, H. Wajant, A. Beilhack, Exogenous TNFR2 activation protects from acute GvHD via host T reg cell expansion. *J. Exp. Med.* **213**, 1881–1900 (2016).
21. X. Chen, J. J. Oppenheim, Targeting TNFR2, an immune checkpoint stimulator and oncoprotein, is a promising treatment for cancer. *Sci. Signal.* **10**, eaal2328 (2017).
22. J. L. Cohen, K. J. Wood, TNFR2: The new Treg switch? *Oncoimmunology* **7**, e1373236 (2018).
23. Y. Nie, J. He, H. Shirota, A. L. Trivett, D. Yang, D. M. Klinman, J. J. Oppenheim, X. Chen, Blockade of TNFR2 signaling enhances the immunotherapeutic effect of CpG ODN in a mouse model of colon cancer. *Sci. Signal.* **11**, eaan0790 (2018).
24. É. S. Vanamee, D. L. Faustman, TNFR2: A novel target for cancer immunotherapy. *Trends Mol. Med.* **23**, 1037–1046 (2017).
25. R. M. Aspalter, M. M. Eibl, H. M. Wolf, Regulation of TCR-mediated T cell activation by TNF-RII. *J. Leukoc. Biol.* **74**, 572–582 (2003).
26. T. Calzascia, M. Pellegrini, H. Hall, L. Sabbagh, N. Ono, A. R. Elford, T. W. Mak, P. S. Ohashi, TNF-α is critical for antitumor but not antiviral T cell immunity in mice. *J. Clin. Invest.* **117**, 3833–3845 (2007).
27. E. Y. Kim, J. J. Priatel, S.-J. Teh, H.-S. Teh, TNF receptor type 2 (p75) functions as a costimulator for antigen-driven T cell responses in vivo. *J. Immunol.* **176**, 1026–1035 (2006).
28. E. Y. Kim, H.-S. Teh, Critical role of TNF receptor type-2 (p75) as a costimulator for IL-2 induction and T cell survival: A functional link to CD28. *J. Immunol.* **173**, 4500–4509 (2004).
29. Y. Agata, A. Kawasaki, H. Nishimura, Y. Ishida, T. Tsubat, H. Yagita, T. Honjo, Expression of the PD-1 antigen on the surface of stimulated mouse T and B lymphocytes. *Int. Immunol.* **8**, 765–772 (1996).
30. T. Powles, J. P. Eder, G. D. Fine, F. S. Braiteh, Y. Loriot, C. Cruz, J. Bellmunt, H. A. Burris, D. P. Petrylak, S.-l. Teng, X. Shen, Z. Boyd, P. S. Hegde, D. S. Chen, N. J. Vogelzang, MPDL3280A (anti-PD-L1) treatment leads to clinical activity in metastatic bladder cancer. *Nature* **515**, 558–562 (2014).
31. R. Dahan, B. C. Barnhart, F. Li, A. P. Yamniuk, A. J. Korman, J. V. Ravetch, Therapeutic activity of agonistic, human anti-CD40 monoclonal antibodies requires selective FcγR engagement. *Cancer Cell* **29**, 820–831 (2016).
32. J. D. Graves, J. J. Kordich, T.-H. Huang, J. Piasecki, T. L. Bush, T. Sullivan, I. N. Foltz, W. Chang, H. Douangpanya, T. Dang, J. W. O'Neill, R. Mallari, X. Zhao, D. G. Branstetter, J. M. Rossi, A. M. Long, X. Huang, P. M. Holland, Apo2L/TRAIL and the death receptor 5 agonist antibody AMG 655 cooperate to promote receptor clustering and antitumor activity. *Cancer Cell* **26**, 177–189 (2014).
33. É. S. Vanamee, D. L. Faustman, Structural principles of tumor necrosis factor superfamily signaling. *Sci. Signal.* **11**, eaao4910 (2018).
34. E. Arduin, S. Arora, P. R. Bamert, T. Kuiper, S. Popp, S. Geisse, R. Grau, T. Calzascia, G. Zenke, J. Kovarik, Highly reduced binding to high and low affinity mouse Fc gamma receptors by L234A/L235A and N297A Fc mutations engineered into mouse IgG2a. *Mol. Immunol.* **63**, 456–463 (2015).
35. M. Lo, H. S. Kim, R. K. Tong, T. W. Bainbridge, J.-M. Vernes, Y. Zhang, Y. L. Lin, S. Chung, M. S. Dennis, Y. J. Y. Zuchero, R. J. Watts, J. A. Couch, Y. G. Meng, J. K. Atwal, R. J. Brezski, C. Spiess, J. A. Ernst, Effector-attenuating substitutions that maintain antibody stability and reduce toxicity in mice. *J. Biol. Chem.* **292**, 3900–3908 (2017).

36. F. Nimmerjahn, S. Gordan, A. Lux, FcγR dependent mechanisms of cytotoxic, agonistic, and neutralizing antibody activities. *Trends Immunol.* **36**, 325–336 (2015).
37. F. Nimmerjahn, J. V. Ravetch, Fcγ receptors as regulators of immune responses. *Nat. Rev. Immunol.* **8**, 34–47 (2008).
38. T. Takai, M. Li, D. Sylvestre, R. Clynes, J. V. Ravetch, FcR γ chain deletion results in pleiotrophic effector cell defects. *Cell* **76**, 519–529 (1994).
39. P. Bruhns, Properties of mouse and human IgG receptors and their contribution to disease models. *Blood* **119**, 5640–5649 (2012).
40. S. Y. Chu, I. Vostiar, S. Karki, G. L. Moore, G. A. Lazar, E. Pong, P. F. Joyce, D. E. Szymkowski, J. R. Desjarlais, Inhibition of B cell receptor-mediated activation of primary human B cells by coengagement of CD19 and FcγRIIb with Fc-engineered antibodies. *Mol. Immunol.* **45**, 3926–3933 (2008).
41. F. Mimoto, H. Katada, S. Kadono, T. Igawa, T. Kuramochi, M. Muraoka, Y. Wada, K. Haraya, T. Miyazaki, K. Hattori, Engineered antibody Fc variant with selectively enhanced FcγRIIb binding over both FcγRIIa^{R131} and FcγRIIa^{H131}. *Protein Eng. Des. Sel.* **26**, 589–598 (2013).
42. A. O. Kamphorst, A. Wieland, T. Nasti, S. Yang, R. Zhang, D. L. Barber, B. T. Konieczny, C. Z. Daugherty, L. Koenig, K. Yu, G. L. Sica, A. H. Sharpe, G. J. Freeman, B. R. Blazar, L. A. Turka, T. K. Owonikoko, R. N. Pillai, S. S. Ramalingam, K. Araki, R. Ahmed, Rescue of exhausted CD8 T cells by PD-1–targeted therapies is CD28-dependent. *Science* **355**, 1423–1427 (2017).
43. M. P. DeBerge, K. H. Ely, P. F. Wright, E. B. Thorp, R. I. Enelow, Shedding of TNF receptor 2 by effector CD8$^+$ T cells by ADAM17 is important for regulating TNF-α availability during influenza infection. *J. Leukoc. Biol.* **98**, 423–434 (2015).
44. J. D. Waight, D. Chand, S. Dietrich, R. Gombos, T. Horn, A. M. Gonzalez, M. Manrique, L. Swiech, B. Morin, C. Brittsan, A. Tanne, B. Akpeng, B. A. Croker, J. S. Buell, R. Stein, D. A. Savitsky, N. S. Wilson, Selective FcγR co-engagement on APCs modulates the activity of therapeutic antibodies targeting T cell antigens. *Cancer Cell* **33**, 1033–1047.e5 (2018).
45. S. A. Quezada, K. S. Peggs, M. A. Curran, J. P. Allison, CTLA4 blockade and GM-CSF combination immunotherapy alters the intratumor balance of effector and regulatory T cells. *J. Clin. Invest.* **116**, 1935–1945 (2006).
46. C. Oderup, L. Cederbom, A. Makowska, C. M. Cilio, F. Ivars, Cytotoxic T lymphocyte antigen-4-dependent down-modulation of costimulatory molecules on dendritic cells in CD4$^+$ CD25$^+$ regulatory T-cell-mediated suppression. *Immunology* **118**, 240–249 (2006).
47. K. Wing, Y. Onishi, P. Prieto-Martin, T. Yamaguchi, M. Miyara, Z. Fehervari, T. Nomura, S. Sakaguchi, CTLA-4 control over Foxp3$^+$ regulatory T cell function. *Science* **322**, 271–275 (2008).
48. S. M. Chin, C. R. Kimberlin, Z. Roe-Zurz, P. Zhang, A. Xu, S. Liao-Chan, D. Sen, A. R. Nager, N. S. Oakdale, C. Brown, F. Wang, Y. Yang, K. Lindquist, Y. A. Yeung, S. Salek-Ardakani, J. Chaparro-Riggers, Structure of the 4-1BB/4-1BBL complex and distinct binding and functional properties of utomilumab and urelumab. *Nat. Commun.* **9**, 4679 (2018).
49. X. Yu, H. T. C. Chan, C. M. Orr, O. Dadas, S. G. Booth, L. N. Dahal, C. A. Penfold, L. O'Brien, C. I. Mockridge, R. R. French, P. Duriez, L. R. Douglas, A. R. Pearson, M. S. Cragg, I. Tews, M. J. Glennie, A. L. White, Complex interplay between epitope specificity and isotype dictates the biological activity of anti-human CD40 antibodies. *Cancer Cell* **33**, 664–675.e4 (2018).
50. J. Polz, A. Remke, S. Weber, D. Schmidt, D. Weber-Steffens, A. Pietryga-Krieger, N. Müller, U. Ritter, S. Mostböck, D. N. Männel, Myeloid suppressor cells require membrane TNFR2 expression for suppressive activity. *Immun. Inflamm. Dis.* **2**, 121–130 (2014).
51. L. Xu, N. Kohli, R. Rennard, Y. Jiao, M. Razlog, K. Zhang, J. Baum, B. Johnson, J. Tang, B. Schoeberl, J. Fitzgerald, U. Nielsen, A. A. Lugovskoy, Rapid optimization and prototyping for therapeutic antibody-like molecules. *MAbs* **5**, 237–254 (2013).
52. R. Levy, C. M. Forsyth, S. L. LaPorte, I. N. Geren, L. A. Smith, J. D. Marks, Fine and domain-level epitope mapping of botulinum neurotoxin type A neutralizing antibodies by yeast surface display. *J. Mol. Biol.* **365**, 196–210 (2007).
53. R. Grantham, Amino acid difference formula to help explain protein evolution. *Science* **185**, 862–864 (1974).

Acknowledgments: We thank B. Bernabe for cell culture work and mycoplasma testing and M. Santiago for work in the animal facility. **Funding:** The laboratory of J.D.M. received funding from Merrimack Pharmaceuticals that partially funded the work. The Marks laboratory was also partially funded by NIH/NCI grant #1P41CA196276-01. **Author contributions:** E.M.T., J.T., V.K., S.K., N.K., K.Z., J.L., J.Q., G.C., Y.J., L.X., V.P., M.R., M.M., and Y.Z. generated, expressed, and characterized proteins and antibodies. J.R., A.C., C.W., A.K., A.-S.D., H.Z., F.D., S.F., J.S., S.G., R.B.F., J.F.S., and J.T. ran the in vivo studies. R.B.F., J.F.S., A.-S.D., A.C., J.R., H.Z., F.D., S.F., and A.J. performed flow cytometry analysis. E.H. scored and annotated the pathology images. L.L. performed the soluble TNFR2 ELISA. W.Q. and A.R. provided support analyzing the data. A.R., E.T., D.C.D., M.M., M.C., and J.D.M. designed the studies. All authors helped write and revise the manuscript. **Competing interests:** As indicated in the affiliations, several coauthors were employees of Merrimack Pharmaceutics at the time of contributing to this work. M.C. and J.D.M. served as paid consultants on the scientific advisory board of Merrimack Pharmaceutics. J.D.M. holds equity in Merrimack Pharmaceuticals. D.C.D. is a stockholder and option holder in Merrimack Pharmaceuticals. At the time the work was being completed, D.C.D. was the Head of Research and Senior Vice President of Merrimack and is currently a consultant of Merrimack. A.R., E.M.T., M.M., D.C.D., A.-S.D., F.D., V.K., and R.B.F. are inventors on provisional patent application #62812859 submitted by Merrimack Pharmaceuticals that covers novel anti-human TNFR2 mAbs. E.T., M.M., J.D.M., Y.Z., and J.S. are inventors on provisional patent application #62812875 submitted by Merrimack Pharmaceuticals and the University of California at San Francisco that covers novel fully human TNFR2 mAbs and their uses. **Data and materials availability:** All data associated with this study are present in the paper or Supplementary Materials. Requests for anti-mouse TNFR2 antibodies (Y9, Y9-DANA, M3, Y7, Y10, and H5L10) can be sent to Merrimack Pharmaceuticals under a material transfer agreement.

Submitted 19 February 2019
Resubmitted 22 May 2019
Accepted 16 August 2019
Published 2 October 2019
10.1126/scitranslmed.aax0720

Citation: E. M. Tam, R. B. Fulton, J. F. Sampson, M. Muda, A. Camblin, J. Richards, A. Koshkaryev, J. Tang, V. Kurella, Y. Jiao, L. Xu, K. Zhang, N. Kohli, L. Luus, E. Hutto, S. Kumar, J. Lulo, V. Paragas, C. Wong, J. Suchy, S. Grabow, A.-S. Dugast, H. Zhang, F. Depis, S. Feau, A. Jakubowski, W. Qiao, G. Craig, M. Razlog, J. Qiu, Y. Zhou, J. D. Marks, M. Croft, D. C. Drummond, A. Raue, Antibody-mediated targeting of TNFR2 activates CD8$^+$ T cells in mice and promotes antitumor immunity. *Sci. Transl. Med.* **11**, eaax0720 (2019).